Water Research 257 (2024) 121660

Contents lists available at ScienceDirect

Water Research

journal homepage: www.elsevier.com/locate/watres

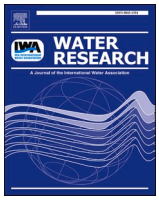

Combined exposure of emamectin benzoate and microplastics induces tight junction disorder, immune disorder and inflammation in carp midgut via lysosome/ROS/ferroptosis pathway

Xu Shi [a], Tong Xu [a], Meichen Gao [a], Yanju Bi [a], Jiaqi Wang [a], Yilin Yin [a], Shiwen Xu [a,b,c,*]

[a] College of Veterinary Medicine, Northeast Agricultural University, Harbin 150030, PR China
[b] Key Laboratory of the Provincial Education Department of Heilongjiang for Common Animal Disease Prevention and Treatment, College of Veterinary Medicine, Northeast Agricultural University, Harbin, 150030, PR China
[c] Laboratory of Embryo Biotechnology, College of Life Science, Northeast Agricultural University, Harbin, 150030, PR China

ARTICLE INFO

Keywords:
EMB
MPs
Carp midgut
Lysosome/ROS
Ferroptosis

ABSTRACT

Pesticides and plastics bring convenience to agriculture and life, but also bring residual pollution in the environment. Emamectin benzoate (EMB) is the most popular pesticide at present. The harm of microplastics (MPs) to water and aquatic organisms is gradually increasing, and the possibility that it appears synchronously with various pesticides increases. However, the damage of EMB and MPs to the carp midgut and its mechanism have not been clarified. Therefore, based on the EMB or/and MPs exposure models, this study explored the mechanism of midgut injury through transcriptomics, immunofluorescence, western blot methods, and so on. Studies *in vivo* and *in vitro* showed that EMB or MPs exposure caused cilia shortening, lysosome damage, and ROS overproduction, which led to Fe^{2+} content increase, GSH/GSSG system disorder, lipid peroxidation, and ferroptosis. This process further led to the down-regulation of Cx43, Occludin, Claudin, and ZO-1, which further caused barrier damage, immune-related genes (immunoglobulin, IFN-γ) decrease and inflammation-related genes (TNF-α, IL-1β) increase. Combined exposure was more significant than that of single exposure, and the addition of EN6 and NAC proved that lysosome/ROS/ferroptosis regulated these midgut damages. In conclusion, EMB or/and MPs exposure induce tight junction disorder, immune disorder and inflammation in carp midgut through the lysosome/ROS/ferroptosis pathway.

1. Introduction

Pesticides play an extremely crucial role in increasing agricultural production and solving human food issues, but they are also the most crucial factors that lead to pesticide pollution to the environment (Gao, Yang et al. 2022, Gao, Zhu et al. 2022). Among them, emamectin benzoate (EMB) is a new high-efficiency semi-synthetic pesticide separated from soil microorganisms, which has the advantages of broad

Abbreviations: EMB, Emamectin benzoate; PS-MPs, MPs, Microplastics; Fe^{2+}, Ferrous iron; GSH, Glutathione; GSSG, Glutathione oxidized; ROS, Reactive oxygen species; Cx43, Connexin43; ZO-1, Zonula occludens 1; IFN-γ, Interferon-γ; IL-1β, 2, 10, Interleukin-1β, 2, 10; TNF-α, Tumor necrosis factor-α; NAC, N-acetyl cysteine; IgM, G, D, Immunoglobulin M, G, D; C3, Complement 3; PE-MPs, Polyethylene microplastics; EPC, Epithelioma papulosum cyprini; CQ, Chloroquine; PBS, Phosphate buffer saline; CCK8, Cell Counting Kit-8; H&E, Hematoxylin and Eosin; AB/PAS, Alixin Blue-Periodic Acid Schiff; IF, Immunofluorescence; CTSB, Cathepsin B; GPx4, Glutathione peroxidase 4; LPO, Lipid peroxide; MDA, Malonaldehyde; H_2O_2, Hydrogen peroxide; CAT, Catalase; SOD, Superoxide dismutase; ACP, Acid phosphatase; NAG, β-N-acetylglucosaminidase; GSH-Px, Glutathione peroxidase; RT-qPCR, Real-time quantitative PCR; LAMP2, Lysosome-associated membrane protein 2; TFR, Transferrin receptor; TF, Transferrin; CXCL8, Chemokine 8; ATP1b3a, ATPase Na^+/K^+ transporting subunit beta 3a; FTHL27, Ferritin heavy polypeptide-like 27; CTSD, Cathepsin D; ATP6V1A, ATPase H^+ transporting V1 subunit A; ATP6V1C2, ATPase H^+ transporting V1 subunit C2; ATP6V1H, ATPase H^+ transporting V1 subunit H; NCOA4, Nuclear receptor coactivator 4; LPCAT3, Lysophosphatidylcholine acyltransferase 3; PTGS2, Prostaglandin-endoperoxide synthase 2; ACSL4, Acyl-CoA synthetase long chain family member 4; SLC3A2, Solute carrier family 3 member 2; GCLC, Glutamate-cysteine ligase catalytic subunit; SLC7A11, Solute carrier family 7 member 11; DMT1, Divalent metal transporter 1; FTH, Ferritin heavy chain 1; FTL, Ferritin light chain; FPN, Solute carrier family 40 member 1; NPs, Nanoplastics; GST, Glutathione S-transferase.

* Corresponding author. College of Veterinary Medicine, Northeast Agricultural University, Harbin, 150030, PR China
E-mail address: shiwenxu@neau.edu.cn (S. Xu).

https://doi.org/10.1016/j.watres.2024.121660
Received 6 November 2023; Received in revised form 30 January 2024; Accepted 21 April 2024
Available online 22 April 2024

insecticidal spectrum, anti-parasite, and long duration, and is the largest selling pesticide at present (Tan, Li et al. 2020). With the increasing application of pesticides causing environmental pollution and residues, its potential toxicity to humans and animals has become increasingly prominent (Shi, Zhu et al. 2022). Firstly, EMB residues were found in the environment. From Nandu River Basin and Wanquan River Basin in Hainan, the detection rate of EMB was 16.14% in 256 topsoil samples, and the highest content was 11.7 μg/kg (Cheng, Van Smeden et al. 2020). In addition, residues of pesticides and herbicides are detected in marine sediments (366 μg/kg w.w.) (Cheng, Van Smeden et al. 2020), surface water (Tan, Zhang et al. 2021) and vegetables (Liu, Sun et al. 2023). In aquatic environments, whether EMB is used as a pesticide or as a parasite prevention drug (St-Hilaire, Cheng et al. 2021), it will cause persistent biological accumulation of EMB in fish or fish-eating organisms. It has been found that the EMB uptake rate constant of *Mytilus edulis* is 4.82, the kinetic bioconcentration factor is 49, and the elimination half-life is as high as 14 days (J, Brooks et al. 2019). Furthermore, EMB has neurotoxicity, developmental toxicity, reproductive toxicity and cardiotoxicity in aquatic animals and mice at low concentrations of acute or chronic exposure (Zhang, Kong et al. 2019, Lu, Wang et al. 2022, Gu, Guo et al. 2023). Exposure to 50 μg/kg EMB increased the expression of IL-1β and TNF-α in the rainbow trout spleen and liver (Kilercioglu, Ay et al. 2020). Exposure to 1 and 2 mg/L EMB induced cardiovascular toxicity of larvae, showing inflammation and apoptosis (Gu, Guo et al. 2023). Exposure to 9.1 μg/L EMB led to a decrease in serum cortisol, immunoglobulin M (IgM) and complement 3 (C3) activities in *L. rohita* fish, which seriously affected the immune function (Kumar, Swain et al. 2022). Although it has been confirmed that EMB can produce toxic effects on a variety of tissues and cells, there are few reports on the toxic mechanism of EMB in carp midgut.

The pollution of polystyrene microplastics (PS-MPs, MPs) has been considered as a major global environmental problem alongside ocean acidification, ozone depletion, and global climate change. MPs has the characteristics of small particle size, stable chemical properties and easy ingestion by aquatic organisms, so it is easy to accumulate and migrate in aquatic organisms and produce biomagnification through the aquatic food chain. The average MPs of 611 particles/kg was detected in the sediments of the Yangtze River valley in China, and the size was less than 1 mm (Yang, Sun et al. 2023). In the Amazon River and its main tributaries, a recent study found that the concentration range of MPs were 5-152 MPs/m^3, and that in urban rivers were 23-74550 MPs/m^3, with a size of 1-5000 μm (Rico, Redondo-Hasselerharm et al. 2023). At present, more than 693 species of marine organisms may eat or eat microplastics by mistake (Gall and Thompson 2015). Sampling was conducted at 210 stations in the western Mediterranean, and it was found that 14.28-15.24% of small pelagic fishes such as *S. pilchardus* and *E. encrasicolus* ingested MPs (Compa, Ventero et al. 2018). 0.68±0.55 MPs/g (1.23±0.99 MPs/shrimp) has been detected in *crangon crangon* (*L.*), a crustacean in the strait area among France, Belgium, the Netherlands and the United Kingdom (Devriese, Van et al. 2015). The ingestion of MPs by aquatic animals will cause a variety of pathological reactions, including inflammation, metabolic pathway changes in the immune system, etc. (Anbumani, Kakkar et al. 2018). Studies have found that MPs exposure leads to inflammation, oxidative stress and energy metabolism disorder in the liver of zebrafish (*Daniorerio*) (Yifeng, Lu et al. 2016). After exposure to 25 and 250 mg/kg MPs for 21 days, the intestinal tight junction of *Sparus aurata Linnaeus* was destroyed, and inflammation and immune response were activated (Del Piano, Lama et al. 2023). In the liver and gill of zebrafish and freshwater bass (*Perca fluviatilis*), 8 and 10 mg/g MPs exposure induced lipid peroxidation, apoptosis and autophagy (Bobori, Feidantsis et al. 2022). In the real water environment, many toxic substances often exist at the same time, which may cause different toxic reactions from those when each substance is exposed alone. After 60 days of exposure to 1.5 or 4.5 mg/L polyethylene microplastics (PE-MPs) and 5 or 15 mg/L glyphosate, the combined exposure damaged the intestinal barrier of carp more than the single exposure (Chen, Rao et al. 2022). In addition, pollutants such as heavy metals (Yan, Hamid et al. 2020, Kang, Byeon et al. 2021, Zhang, Li et al. 2022), nano-plastics (Kang, Byeon et al. 2021) and acetochlor (Wang, Zhao et al. 2023) were also found to have joint toxic effects with MPs.

At present, EMB and MPs are exposed to aquatic animals, and induce inflammation and immune damage in tissues and organs (Gall and Thompson 2015, Kilercioglu, Ay et al. 2020, Del Piano, Lama et al. 2023). Fish is a model organism in toxicology experiments (Zhao, Wang et al. 2021), among which carp (*Cyprinus carpio*) has the advantages of large scale, strong adaptability and easy acquisition (Zhao, Zhang et al. 2023). Ferroptosis is a new type of iron-dependent programmed cell death, which is closely related to intestinal inflammation and immune function (Subramanian, Geng et al. 2020). Current research declares that both endoplasmic reticulum and mitochondria can mediate the process of ferroptosis (Krainz, Gaschler et al. 2011, Doll, Proneth et al. 2016). Lysosomal dysfunction has a profound impact on cell homeostasis, which will lead to the increase of ROS and the damage of mitochondria and other organelles (Patricia, Antioxidants et al. 2012). However, whether EMB or MPs will increase ROS through lysosomal injury, whether it will further induce the increase of intestinal permeability, inflammation and immune dysfunction of carp by causing ferroptosis, and whether EMB and MPs will have joint toxic effects are unknown. Therefore, in this study, the EMB or/and MPs exposure models in carp midgut and EPC cells were constructed to explore: (1) Whether pesticides and MPs are geographically co-occurring. (2) Whether EMB or MPs exposure would cause ferroptosis by activating the lysosome/ROS pathway. (3) Whether EMB or MPs exposure would destroy the intestinal barrier, inflammation and immune damage in carp midgut. (4) Whether the combined exposure of EMB and MPs would have more obvious toxicity than the single exposure. The joint exposure of multiple pollutants is more practical than the study of single pollutant exposure and has a strong guiding significance for actual water environment protection.

2. Materials and Methods

2.1. Carp grouping, EMB or/and MPs exposure model establishment

The animal welfare in the whole experiment strictly abides by the standards of the Committee for the Protection and Use of Laboratory Animals of Northeast Agricultural University and the EU Directive on the Protection of Laboratory Animals (SM-11). Sixty healthy carp (206.34 ± 8.63 g) from a fish farm in Changling Lake, Harbin were randomly raised in a barrel (60 cm × 30 cm × 26 cm) filled with 15 L water, with 5 carp per barrel (n=3). After a week of adaptation, the carp were randomly divided into four groups: control group (C), EMB group, MPs group and EMB+MPs group. The content of EMB (E396669, purity>95%, Aladdin) is 2.4 μg/L in water (Kumar, Swain et al. 2022), and the content of MPs (PS-MPs, 10 μm, Fengtai polymer material) water is 500 μg/L in water (Ouyang, Liu et al. 2021). Feeding twice a day, replacing half of the water in the water tank with dechlorinated tap water, and adding EMB and MPs to the water body according to the dose. No carp died within 30 days of the acute toxicity test. On the 31st day, all carp were euthanized, and midgut was collected immediately. Some midgut samples were fixed in 4% paraformaldehyde. A part of 0.9% NaCl added with ice was made into tissue homogenate for kit detection. The remaining samples were stored in liquid nitrogen at -80°C for transcriptomics, qRT-PCR and western blot analysis.

2.2. Map distribution map

To understand the residue of MPs in the world, we searched 843 articles with keywords of "microplastics", "water" and "soil" in NCBI (https://www.ncbi.nlm.nih.gov/) from 2018 to 2023, further filtered them according to their titles and abstracts, and finally collected the

data of 204 studies, and summarized the continents, countries, and samples (Table S1) to the geographical distribution map of MPs residue. In addition, the global pesticide usage per cultivated area in 2021 (Table S2) was obtained from the website of the Food and Agriculture Organization of the United Nations (https://www.fao.org/) to draw the geographical distribution map of pesticide usage.

2.3. EPC cells treatment

Epithelioma papulosum cyprini (EPC) cell was cultured in L15 (11415064, Gibco) complementary with 10% FBS (1705124, VivaCell, Shanghai, China) and 1% penicillin-streptomycin-amphotericin B solution (Beyotime, China), and held at 28°C without CO_2. When the density of EPC cells reached 100%, the cells were passaged, and the 3rd-8th generation EPC cells were selected for the follow-up experiment.

2.4. Agent configuration and viability assay by CCK8 method

The EMB solid was dissolved in DMSO (Solarbio, China) to obtain an initial concentration of 1 mM, and then diluted with culture medium to obtain the target concentration of 0, 0.1, 0.5, 1, 2, 3, 4, 5, 7, 8, 10 μM, respectively. The MPs solid was configured in phosphate buffer saline (PBS) to obtain an initial concentration of 10 mg/mL, and then diluted with culture medium to obtain the target concentration of 0, 0.1, 1, 10, 50, 100, 200, 400, 500, 600, 800, and 1000 μg/mL, respectively. N-acetyl cysteine (NAC, A7250, Sigma) solid was dissolved in DMSO to attain 1 M initial density and 1 mM target concentration. Chloroquine (CQ, 54-05-7, MCE) solid was dissolved in DMSO to attain 1 mM initial density and 20 μM target concentration. EN6 (1808714-73-9, MCE) solid was dissolved in DMSO to attain 10 mM initial density and 15 μM target concentration.

The Cell Counting Kit-8 (CCK-8) method was used to assess the toxic effect of EMB or/and MPs on EPC cells. 8×10^3 cells were planted in each well of 96-well plate, and EPC cells were cultured with different concentrations of EMB or/and MPs for 24 h. Then working solution with 10% CCK-8 (40203ES80, Yeasen) was cultured for another 2.5 h at 28°C. Afterwards, Multiskan SkyHigh (Thermo) was used to examine the absorbance at 450 nm.

2.5. Hematoxylin and Eosin (H&E), Alixin Blue-Periodic Acid Schiff's (AB/PAS) staining, and histopathological score

To assess the influence of EMB or/and MPs exposure on midgut tissue structure and mucus. The midgut fixed in 4% paraformaldehyde was made into slices, with three sheets per group. Then, the sections in C, EMB, MPs, and EMB+MPs groups were H&E and AB/PAS staining according to Li's research (Li, Hu et al. 2022). The slices were photographed by CaseViewer software, and the length of cilia (μm) and the depth of recess (μm) were measured.

Three researchers used the blind method to score the H&E staining of the midgut in C, EMB, MPs and EMB+MPs groups. According to Liu's research (Liu, Wang et al. 2021), the histopathological scoring standard for the midgut was improved to score five aspects in terms of changes of cilia length and quantity, degree of inflammation, infiltration depth of inflammatory cells, damage degree of recess, and lesion range, as described in Table S3. The theoretical score range was 0~16 points.

2.6. Transcriptomics

The TRIzol method was used to extract total RNA from carp midgut. The concentration and purity of total RNA were measured by NanoDrop spectrophotometer (Thermo) and Labchip GX Touch HT Nucleic Acid Analyzer (PerkinElmer, USA) respectively. High-quality total RNA was sent to Wuhan Bioacme Biotechnology Company (Wuhan, China) for cDNA library construction and sequencing, and mRNA was enriched with oligo (dT) beads. According to the manufacturer's protocol, the RNA sequencing library was generated by making use of the KAPA strand RNA-Seq kit of illumina with multiple primers. Then it was sequenced on the illumina Nova sequencer. Subsequently, we constructed the gene library and analysed the differential expression. Additionally, we used the Lianchuan bioanalysis platform to make a GO string diagram, annular heat diagram, circle diagram, multi-group differential volcano diagram and GSEA enrichment analysis.

2.7. Immunofluorescence staining of midgut and EPC cells

To examine the mechanism of EMB or/and MPs toxic effects, we performed single or double immunofluorescence staining (IF) on midgut and EPC cells. Refer to Shi's article (Shi, Zhu et al. 2022), primary antibodies were CTSB (1:200, Abclonal), GPx4 (1:100, Abclonal), Cx43 (1:100, Abclonal), TNF-α (1:100, Abcam), and IL-1β (1:100, Abcam). Secondary antibodies were Dlight 594 and Dlight 488 (1:500, Biodragon), and DAPI staining (DA0004, Leagene) was used to display the nuclei of EPC cells. Images were collected by an inverted fluorescence microscope (Olympus, IXplore). Image J was used to quantify the total red or green fluorescence intensity of $CTSB^+$, $GPx4^+$, $Cx43^+$, $TNF\text{-}\alpha^+$ and $IL\text{-}1\beta^+$ on EPC cells.

2.8. Detection of iron ion (Fe^{2+}) content in the midgut and EPC cells

The midgut tissues were homogenised in 0.9% NaCl, and the treated EPC cells were collected with 0.9% NaCl and centrifuged (4℃, 3500 r/min, 15 min). According to the instruction, the supernatant was used to analyze the Fe^{2+} content (A039-2-1, Nanjing Jiancheng Bioengineering Institute).

2.9. Detection of oxidative stress and lipid peroxide (LPO)

The samples of midgut and EPC cells in C, EMB, MPs and EMB+MPs groups were prepared as in 2.8. According to the instruction, the supernatant was used for the detection of malonaldehyde content (MDA, A039-2-1), hydrogen peroxide content (H_2O_2, A064-1-1), catalase activity (CAT, A007-1-1), LPO content (A106-1-1), and superoxide dismutase activity (SOD, A001-1-2), which purchased from Nanjing Jiancheng Bioengineering Institute.

2.10. Detection of lysosomal enzyme activity in midgut and EPC cells

The samples of midgut and EPC cells in C, EMB, MPs and EMB+MPs groups were prepared as in 2.8. According to the instruction, the supernatant was used for the detection of acid phosphatase (ACP, A060-1-1) and β-N-acetylglucosaminidase (NAG, A031-1-1) activities, which all purchased from Nanjing Jiancheng Bioengineering Institute.

2.11. Detection of glutathione/glutathione oxidized (GSH/GSSG) system

The samples of midgut and EPC cells in C, EMB, MPs and EMB+MPs groups were prepared as in 2.8. According to the instruction, the supernatant was used for the detection of glutathione peroxidase (GSH-Px, A005-1-2, Nanjing Jiancheng), GSH and GSSG content (A061-2-1, Nanjing Jiancheng).

2.12. Detection of ROS by DCFH-DA staining

EPC cells were treated with EMB or/and MPs according to 2.4 for 24 h. The green fluorescence levels of EPC cells were labelled with a Reactive Oxygen Species Assay Kit (E004-1-1, Nanjing Jiancheng). Next, the ROS images of EPC cells were captured by fluorescence microscope and the relative green fluorescence intensity of C, EMB, MPs and EMB+MPs groups were quantified and compared by Image J.

2.13. Detection of Fe^{2+} by FerroOrange staining

EPC cells were treated according to 2.4 for 24 h. The red fluorescence level of Fe^{2+} in EPC cells was labelled with 1 μM FerroOrange Fluorescent Probe (MX4559, MKBio) for 20 min at 28℃. The red fluorescence of Fe^{2+} was captured when the emission wavelength was 572 nm and the excitation wavelength was 488 nm, and the total fluorescence intensity was quantified and compared by Image J software.

2.14. Detection of Lysosome number

EPC cells were treated according to 2.4 for 24 h. We prepared 50 nM Lyso-Tracker Red (C1046, Beyotime) working solution and Hoechst 33342 staining solution (C1025, Beyotime) and added them to EPC cells in treatment groups. Next, the lysosome images of EPC cells were captured by fluorescence microscope and the relative fluorescence intensity of treatment groups were quantified and compared by Image J.

2.15. Detection of lipid peroxidation on EPC cells

EPC cells were treated according to 2.4 for 24 h. To evaluate lipid peroxidation, the treated EPC cells were cultured with 5 μM C11 BODIPY 581/591 (MX5211, MKBio) for 20 min at 28℃, and then the captured fluorescence images were detected at 488 nm and 594 nm. In short, C11 BODIPY 581/ 591 is essentially a lipophilic dye, and the oxidized lipid shows green fluorescence, while the unoxidized lipid shows red fluorescence. The total fluorescence intensity was quantified and compared by Image J software.

2.16. Total RNA extraction, reverse transcription and real-time quantitative PCR (RT-qPCR)

We used RT-qPCR to examine the transcription levels of target genes in the midgut and EPC cells. Referring to the previous study (Miao, Miao et al. 2023, Wang, Liu et al. 2023), total RNA was obtained by the TRIzol method from the midgut and EPC cells. After determining the purity and concentration of RNA, we reversed transcribed total RNA into cDNA (MR05101M, Monad), and used SYBR Green fluorescent dye (AQ132-11, Transgen) for quantitative detection in the Roche LightCycler®96 system. The primers of CTSB, Cx43 and other gene primers used in this study were shown in Table S4. β-actin played a part in the endogenous controls for the goal of normalization. The $2^{-\Delta\Delta CT}$ method was used to calculate the target gene levels.

2.17. Total protein extraction and western blot analysis

We visualized the protein level of the following indicators in the midgut and EPC cells by using the western blot technique. The specific method of western blot refers to Miao's study (Miao, Miao et al. 2022). The antibodies needed in this study were CTSB (1:1000, Abclonal), CTSD (1:500, Wanleibio), LAMP2 (1:500, Wanleibio), GPx4 (1:1000, Abclonal), TFR (1:500, Wanleibio), TF (1:1000, Wanleibio), Cx43 (1:1000, Abclonal), Occludin (1:1000, Wanleibio), Claudin (1:1500, Wanleibio), ZO-1 (1:1000, Wanleibio), IL-2 (1:1000, CST), IFN-γ (1:500, Wanleibio), and β-actin (1:5000, Bioss). The second antibody conjugated with peroxidase of anti-rabbit and anti-mouse IgG (1:100000, Immunoway) was incubated for 1-2 h at 25℃. Finally, the semaphore was evaluated by the Super ECL Kit (MA0186, Meilunbio). Image J was used to quantify these protein bands.

2.18. Statistical analyses

All the results of in midgut and EPC cells were analyzed and displayed through GraphPad Prism 8. All data was denoted as the mean ± the standard error of the mean (SEM). We carried out the Shapiro-Wilk Normality test in the midgut and EPC cells and found that these results traversed the normality test (alpha=0.05). For One-Way ANOVA, Tukey's post-hoc multiple comparisons in GraphPad Prism 8 were used to analyze the significance of differences between every two groups. The same letter represents no significant difference ($P > 0.05$); completely different letters represent a significant difference ($P < 0.05$).

3. Results

3.1. Pesticides and MPs are geographically co-occurring in the world

Through preliminary data screening, we found that the global pesticide consumption per cultivated land (Fig. 1A) and pesticide residues in MPs environment (Fig. 1B) were co-occurrences in geographical distribution. Among them, the five countries with the highest use of pesticides (per unit area) were Brunei Darussalam, Saint Lucia, New Caledonia, Trinidad and Tobago and, Hong Kong SAR, China. The five countries with the highest frequency of MPs residues reports were China, Germany, Iran, India, Canada and Spain. In the seven continents statistics, Asia and Europe were the most areas per unit area of cultivated land (Fig. 1C-D) and MPs environmental residues reported (Fig. 1E). EMB is one of the most widely used pesticides, so we speculated that EMB and MPs had co-occurrence in geographical space.

3.2. Effect of EMB or/and MPs exposure on midgut histomorphology of carp and confirmation of exposure concentration in vitro

Firstly, the effects of EMB and MPs on the midgut histomorphology of carp were observed by H&E staining, as shown in Fig. 2A. In the C group, the structure of mucosal muscularis and intestinal villi was intact, and there were fewer inflammatory cells. Compared with the C group, EMB group and MPs group showed structural disorder of mucosal muscularis, and intestinal villi became shorter and less, accompanied by infiltration with inflammatory cells (yellow arrows). In the EMB+MPs group, intestinal villi became thinner and less. Histopathological score (Fig. 2B), cilia length (Fig. 2C), crypt depth (Fig. 2D) and VCR ratio (Fig. 2E) also showed that EMB or MPs group induced damage to midgut tissue structure and cilia, and the damage was aggravated in the EMB+MPs group. In addition, AB/PAS staining displayed that compared with the C group, goblet cells (purple granules) in EMB group and MPs group decreased significantly, and some ciliated purple granules in EMB+MPs group almost disappeared (Fig. 2F). Then, in Fig. 2G-H, we detected the effect of EMB or MPs on EPC cell viability by CCK8 method. With the increase of EMB or MPs concentration, EPC cell viability decreased. We chose 2.5 μM EMB and 450 μg/mL MPs as the exposure dose of this experiment *in vitro* according to the combined exposure of EMB and MPs (Fig. 2I). In Fig. 2J, we calculated IC_{50} of EMB and MPs to EPC cells as 4.765 μM and 1480.8 μg/mL, respectively. The above results reveal that EMB or/and MPs induce the integrity of midgut tissue structure and cilia damage of carp.

3.3. Results of EMB or/and MPs exposure on midgut transcriptomics of carp

To clarify the influence of EMB or/and MPs on carp midgut, the transcriptome analysis of midgut tissue was carried out in this experiment. Venn diagram displayed that 21 genes in carp midgut were differentially expressed among five groups analysis (Fig. 3A). Compared with the control group, EMB exposure caused 1256 genes to be up-regulated and 1111 genes to be down-regulated. MPs exposure caused 745 genes to be up-regulated and 833 genes to be down-regulated. We screened the annotated differential genes to make several groups of differential volcanic maps. The results showed that the expressions of genes such as CTSB, ILs, ATP1b3a, FTHL27, and TNF were up-regulated, while GPx4, Cx43, Claudin, and CXCL8 were down-regulated (Fig. 3B). KEGG analysis manifested that EMB exposure also resulted in differential enrichment of lysosome, fatty acid metabolism, glutathione

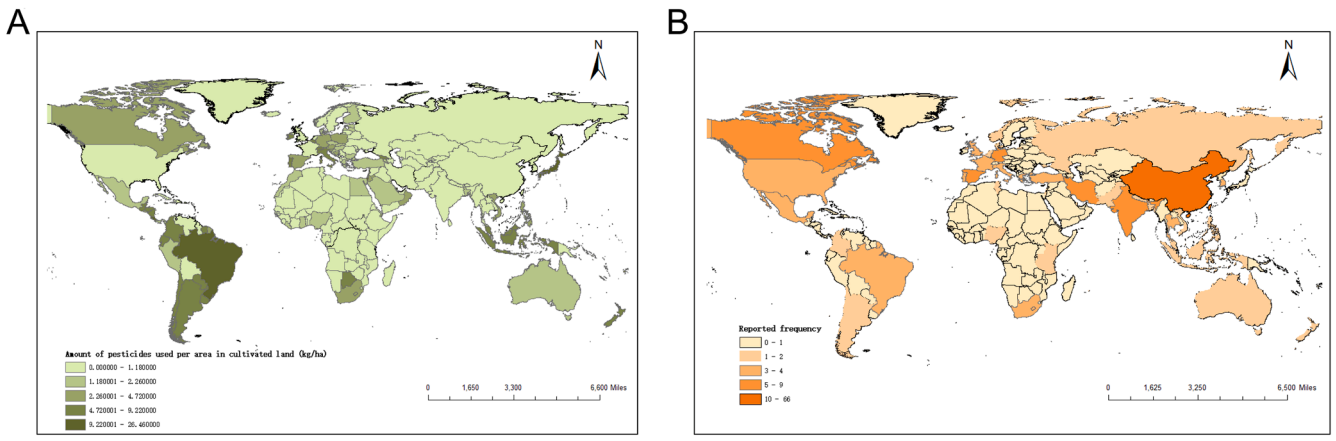

C

Table1 The amount of pesticides used per cultivated area in all continents (2021)

Continent	Amount of pesticides used per area in cultivated land (kg/ha)
Asia	182.89
Europe	134.51
Oceania	107.39
Africa	68.56
South America	77.63
North America	131.21
Latin America	8.51

D

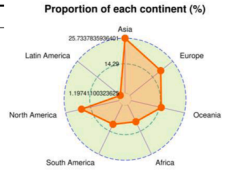

E

Table2 Report frequency of MPs environmental residues in various continents.

Continent	Reported frequency
Asia	116
North America	16
Europe	52
Oceania	4
Africa	15
South America	9
Antarctica	1

Fig. 1. Geographical distribution map of pesticide consumption per cultivated land and residue reports in MPs environment (A) Global pesticide consumption per cultivated land (kg/ha). (B) Frequency of each country in 204 MPs environmental residue reports. (C) The amount of pesticides used per cultivated area in all continents (2021). (D) Proportion of pesticide use per unit area of cultivated land in each continent (%). (E) Report frequency of MPs environmental residues in various continents.

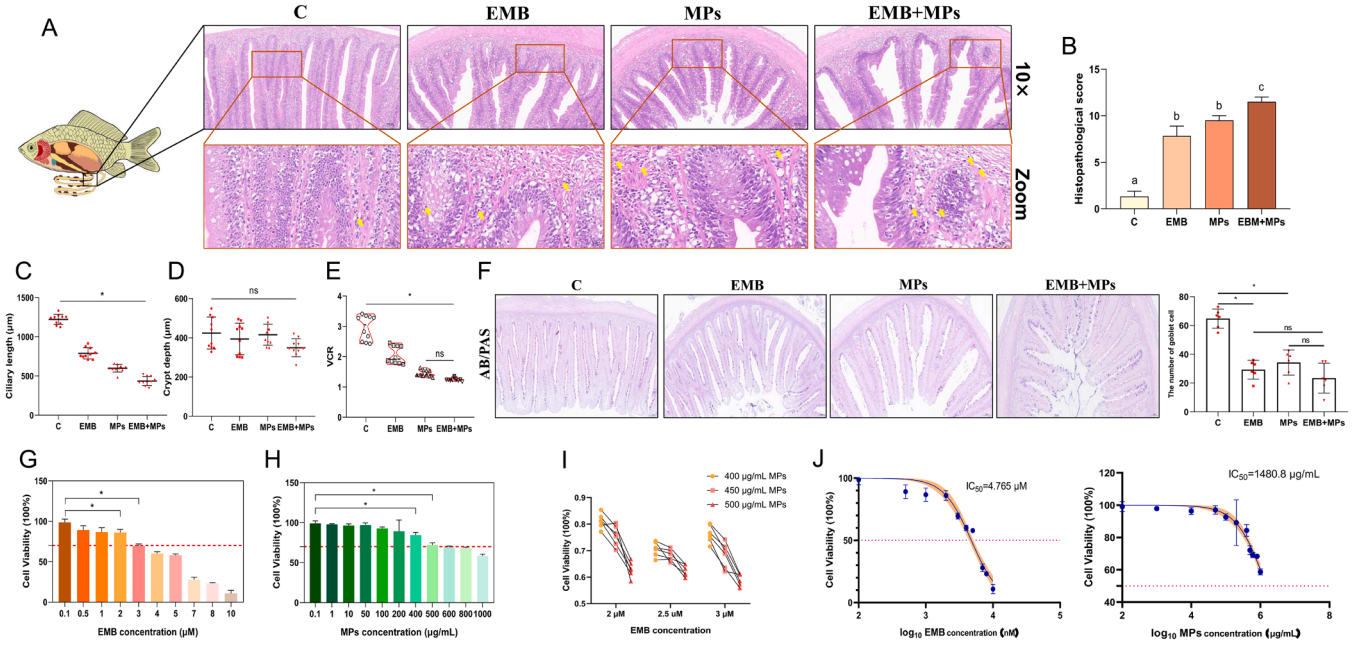

Fig. 2. Observation on midgut structure of carp and dose confirmation of EPC cells exposed to EMB or /MPs (A) H&E staining results of midgut in the C, EMB, MPs and EMB+MPs groups (n=3). The scale of low-power lens (10×) is 100 μm. The scale of high-power lens (Zoom) is 20 μm. (B) The histopathological score was scored by H&E staining (n=3). (C) Based on the results of H&E staining, the length of midgut cilia (μm) was measured (n=10). (D) Based on the results of H&E staining, the depth of midgut crypt (μm) was measured (n=10). (E) The ratio of cilia length to crypt depth (VCR) on midgut. (F) AB/PAS staining and the number of goblet cell (every cilia) in the C, EMB, MPs and EMB+MPs groups (Scale, 100 μm). (G) The viability of EPC cells was treated with different concentrations (0, 0.1, 0.5, 1, 2, 3, 4, 5, 7, 8 and 10 μM) of EMB for 24 h (n=5). (H) The viability of EPC cells was treated with different concentrations (0, 0.1, 1, 10, 50, 100, 200, 400, 500, 600, 800 and 1000 μg/mL) of MPs for 24 h (n=5). (I) The viability of EPC exposed to EMB (2, 2.5, 3 μM) and MPs (400, 450, 500 μg/mL) for 24 h (n=5). (J) The IC_{50} of EMB and MPs was calculated by nonlinear equation. "*" represents a remarkable difference from the control group ($P<0.05$).

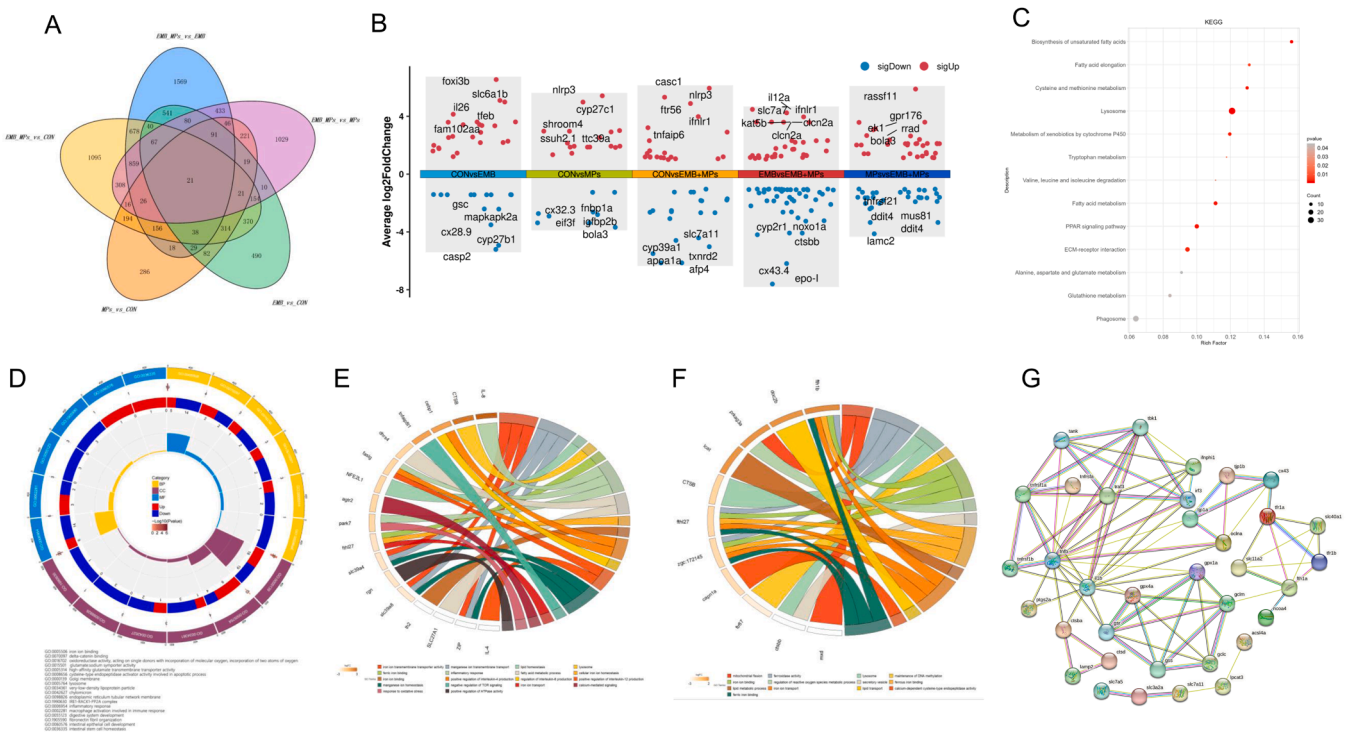

Fig. 3. Transcriptome results of carp midgut exposed to EMB or /MPs (A) The Venn diagram showed the distribution of differentially expressed genes exposed to EMB or/and MPs (n=3). (B) The multiple groups of differential volcanic maps showed the distribution of differentially expressed genes up-regulated and down-regulated exposed to EMB or/and MPs (n=3). (C) The analysis results of KEGG enrichment in EMB vs CON (n=3). (D) The radar chart in MPs vs CON showed GO analysis results (n=3). (E) The chord diagram in EMB+MPs vs CON showed GO analysis results (n=3). (F) The chord diagram in EMB+MPs vs EMB showed GO analysis results (n=3). (G) The Protein-Protein Interaction Networks (PPi) of related genes in transcriptomics results.

metabolism, and phagocyte (Fig. 3C). Radar diagram showed that MPs exposure also induced inflammation response, macrophage activation, intestinal epithelial cell development and intestinal stem cell homeostasis (Fig. 3D). GO enrichment chord diagram showed that EMB and MPs exposure caused significant enrichment of lysosomes, fatty acid metabolism process, inflammation response, iron ion transport and response to oxidative stress (Fig. 3E). Compared with the single exposure, the combined exposure is also differentially enriched to the process of iron ion binding and lipid metabolism (Fig. 3F). In Fig. 3G, the interaction among lysosomes, glutathione metabolism, iron metabolism, oxidative stress, inflammation, immune response and gap junction was found through PPi interaction network.

3.4. EMB or/and MPs exposure induced lysosome damage in carp midgut and EPC cells

Based on screening the expression of lysosome-related genes from the transcriptomics results (Fig. 4a), we investigated the function of EMB or/and MPs exposure on the midgut of carp (Fig. 4A). In Fig. 4b, the red fluorescence of $CTSB^+$ in EMB group and MPs group, compared with the control group, increased obviously, and changed from punctate to diffuse (yellow arrow), and the fluorescence intensity of $CTSB^+$ in EMB+MPs group more increased. The transcription and protein levels of CTSB and CTSD in the EMB group or MPs group were significantly up-regulated (Fig. 4c-d), while LAMP2 was significantly down-regulated, and the changes of these three genes in EMB+MPs group were more significant ($P < 0.05$). Additionally, the levels of lysosomal V-ATPase pump-related genes (ATP6V1A, ATP6V1C2 and ATP6V1H) decreased after EMB or MPs exposure ($P < 0.05$), while the EMB+MPs group decreased to about half of that in the C group (Fig. 4e). This shows that EMB or/and MPs lead to lysosomal acidification damage. In Fig. 4f, lysosomal enzyme activities (ACP and NAG) in EMB+MPs group were significantly smaller than those in EMB group, MPs group, and C group ($P < 0.05$). Nuclear receptor coactivator 4 (NCOA4) is involved in the regulation of ferritin phagocytosis as a selective loading receptor of ferritin. In Fig. 4g, we found that the expression level of NCOA4 in EMB group or MPs group decreased significantly, and further decreased in EMB+MPs group ($P < 0.05$). The above data suggest that EMB or MPs leads to lysosomal damage, and the combined exposure further aggravates the damage.

Subsequently, we verified the effects of EMB or/and MPs on lysosomal injury in EPC cells (Fig. 4B). The red fluorescence of $CTSB^+$ (Fig. 4h-i) in EMB group or MPs group increased significantly and changed from punctate to diffuse, and the number of lysosomes (Fig. 4j-k) decreased significantly ($P < 0.05$). These data changes in EMB+MPs group were more obvious than that of the single exposure group. In Fig. 4l-m, EMB+MPs group had higher transcription and protein levels of CTSB and CTSD and lower level of LAMP2 than the EMB group or MPs group ($P < 0.05$). In addition, lysosomal enzyme activities (ACP and NAG) also gradually decreased with a single exposure and combined exposure (Fig. 4n). The expression of ATP6V1A, ATP6V1C2 and ATP6V1H in the exposed group all tended to be down-regulated (Fig. 4o). Among them, the expression of ATP6V1H in EMB+MPs group decreased significantly ($P < 0.05$). The expression of NCOA4 was similar to that *in vivo*, that is, EMB or/and MPs exposure caused the down-regulation of NCOA4 expression (Fig. 4p). The above results show that EMB or/and MPs cause the acidification of lysosomes, the decrease of enzyme activity and the decrease of lysosomes number.

3.5. EMB or/and MPs exposure mediated oxidative stress, lipid peroxidation and GSH/GSSG system

The results of transcriptomics GSEA analysis demonstrated that oxidative stress-related processes were enriched among the C, EMB, MPs and EMB+MPs groups (Fig. 5A). In Fig. 5B, we also screened the expression of genes related to lipid metabolism, but not all the genes

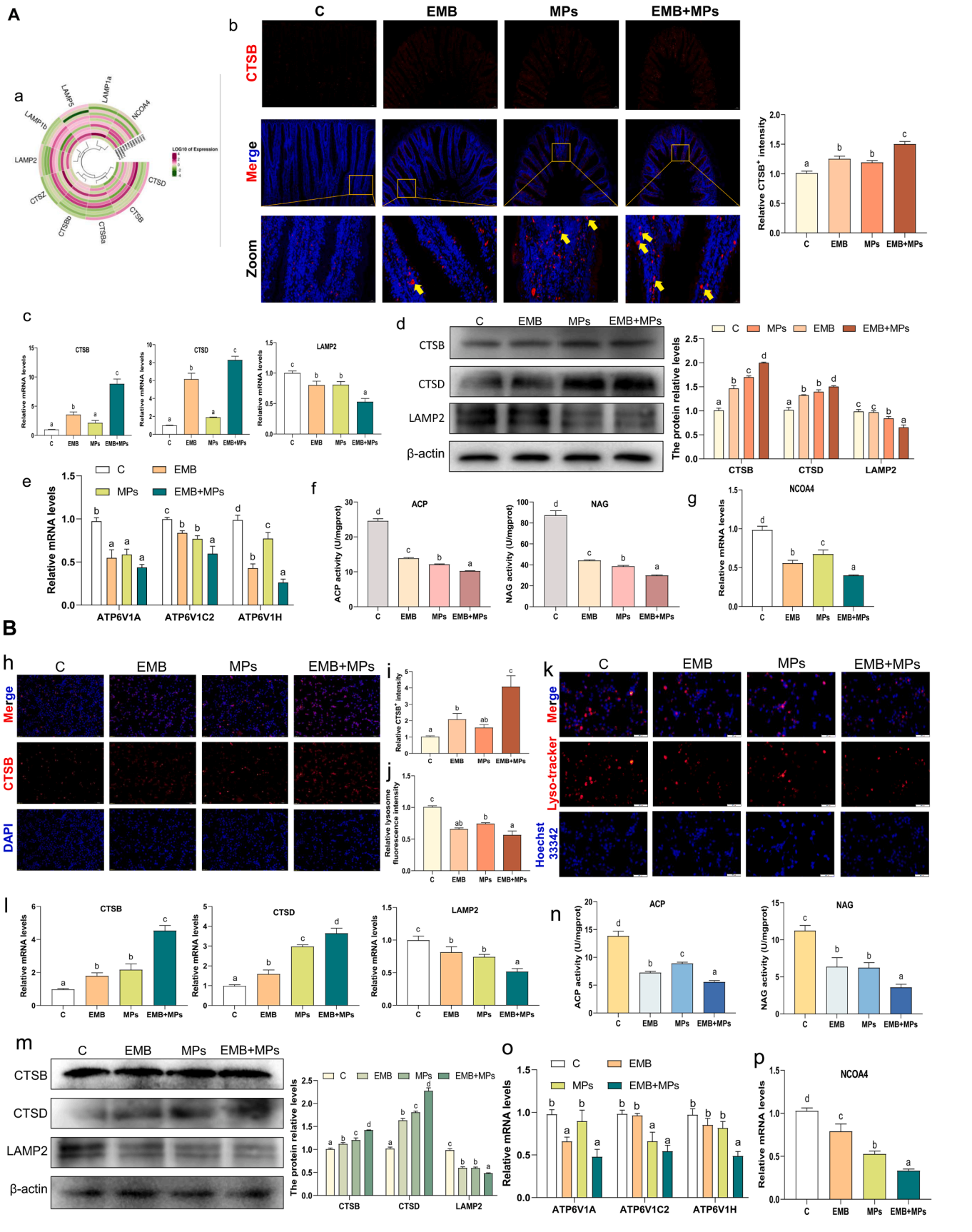

(caption on next page)

Fig. 4. Effects of EMB or/and MPs exposure on lysosome injury
A (a) The cyclic thermogram of lysosome related gene expression in transcriptomics (n=3). (b) IF results and quantification of CTSB (Red) in midgut tissue. DAPI (Blue) stained nuclei (Scale, 100 μm and 20 μm). (c) The mRNA levels of CTSB, CTSD, and LAMP2 (n=3). (d) The protein expression and quantitative graphs of CTSB, CTSD, and LAMP2 (n=3). (e) The mRNA levels of ATP6V1A, ATP6V1C2, and ATP6V1H (n=3). (f) The activities of ACP and NAG (U/mgprot) in midgut tissue (n=3). (g) The mRNA levels of NCOA4 (n=3).
B (h, i) IF results and quantification of CTSB (Red) in EPC cells. DAPI (Blue) stained nuclei (Scale, 200 μm). (j, k) Lyso-tracker (50 nM) and Hoechst 33342 stained lysosome and nuclei of EPC cells. (Scale, 100 μm). (l) The mRNA levels of CTSB, CTSD, and LAMP2 (n=3). (m) The protein expression and quantitative graphs of CTSB, CTSD, and LAMP2 (n=3). (n) The activities of ACP and NAG in EPC cells (n=3). (o) The mRNA levels of ATP6V1A, ATP6V1C2, and ATP6V1H (n=3). (p) The mRNA levels of NCOA4 (n=3).

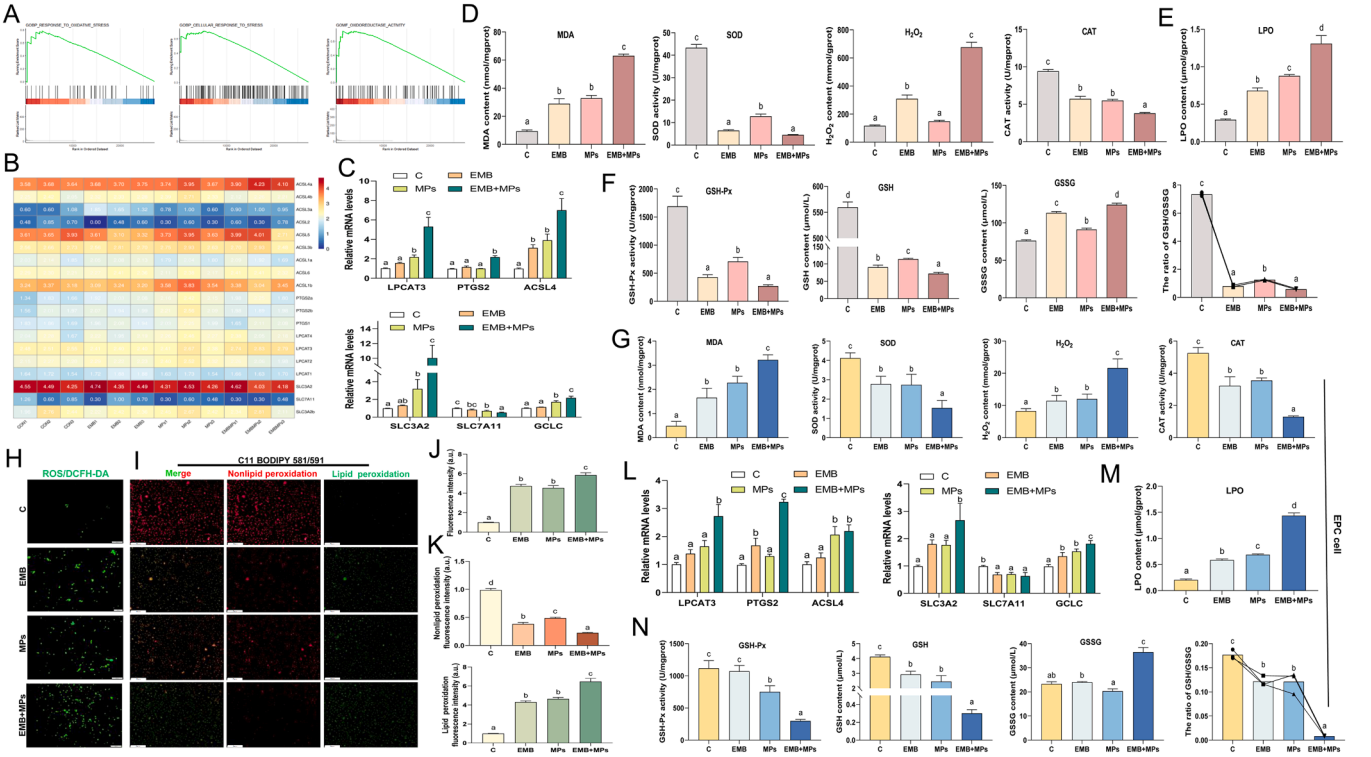

Fig. 5. Effects of EMB or/and MPs exposure *in vivo* and *in vitro* on oxidative stress, lipid peroxidation and GSH/GSSG system (A) The results of GSEA enrichment in transcriptomics of carp midgut. (B) The heat map results of lipid metabolism related genes in transcriptomics. (C) The mRNA levels of LPCAT3, PTGS2, ACSL4, SLC3A2, SLC7A11, and GCLC in midgut tissue (n=3). (D) The content of MDA (nmol/mgprot) and H_2O_2 (mmol/mgprot) and the activities of SOD and CAT (U/mgprot) in midgut tissue (n=4). (E) The content of LPO (μmol/mgprot) in midgut tissue (n=4). (F) The activity of GSH-Px (U/mgprot), the content of GSH and GSSG (μmol/L) and the ratio of GSH/GSSG in midgut tissue (n=3). (G) The content of MDA and H_2O_2 (mmol/mgprot) and the activities of SOD and CAT in EPC cells (n=4). (H) The detection of ROS level (Green) in EPC cells by DCFH-DA staining (n=3) (Scale, 100 μm). (I) The detection of lipid peroxidation in EPC cells by C11 BODIPY 581/591 (5 μM) staining (n=3). The unoxidized lipid was red, and the oxidized lipid was green (Scale, 100 μm). (J) Quantification of total fluorescence intensity of ROS in EPC cells (n=3). (K) Quantification of lipid peroxidation and non-lipid peroxidation fluorescence intensity in EPC cells (n=3). (L) The mRNA levels of LPCAT3, PTGS2, ACSL4, SLC3A2, SLC7A11, and GCLC in EPC cells (n=3). (M) The content of LPO in EPC cells (n=4). (N) The activity of GSH-Px, the content of GSH and GSSG and the ratio of GSH/GSSG in EPC cells (n=3).

were significantly different ($P > 0.05$). Based on the important role of lipid peroxidation products in ferroptosis, we measured the mRNA levels of LPCAT3, PTGS2 and ACSL4 (Fig. 5C). The transcription levels of the above genes in EMB+MPs group were larger than those in EMB group, MPs group and C group ($P < 0.05$). In addition, the contents of MDA, H_2O_2 and lipid peroxide (LPO), compared with the control group, in EMB group and MPs group enhanced, while the activities of SOD and CAT declined ($P < 0.05$), the EMB+MPs group also further changed (Fig. 5D-E). Subsequently, we detected the changes in the GSH metabolic pathway. From the aspect of glutamic acid transport (Fig. 5C), we found that the transcription levels of SLC3A2 and GCLC in the EMB group or MPs group up-regulated, while SLC7A11 decreased, and the changes in EMB+MPs group were the most significant ($P < 0.05$). In terms of GSH/GSSG system (Fig. 5F), GSH-Px activity and GSH content in EMB group or MPs group decreased significantly, while the GSSG content increased, and the GSH/GSSG ratio decreased precipitously ($P < 0.05$). The above indexes in EMB+MPs group changed further, but there was no significant difference in some indexes. These results indicate that EMB or/and MPs induce oxidative stress, lipid peroxidation and GSH/GSSG system disorder in carp midgut.

We verified the above results with EPC cells *in vitro*. The contents of MDA and H_2O_2 raised, while the activities of SOD and CAT decreased ($P < 0.05$), especially in EMB+MPs group (Fig. 5G). The results of ROS content in EPC cells exhibited that the green fluorescence intensity of EMB+MPs group was higher than that of EMB group, MPs group and C group (Fig. 5H and 5J). Using C11 BODIPY 581/591 to dye the lipid that has unoxidized (red) or oxidized (green), it was found that the green fluorescence increased and the red fluorescence decreased obviously in EMB group or MPs group, and the proportion of green fluorescence in EMB+MPs group further increased (Fig. 5I and 5K). In Fig. 5L, the transcription levels of LPCAT3, PTGS2, ACSL4, SLC3A2, and GCLC in EMB group and MPs group were significantly increased, while SLC7A11 was significantly decreased ($P < 0.05$). EMB+MPs group showed a trend of further changes, but there was no significant difference in ACSL4 and

SLC7A11 ($P > 0.05$). LPO content *in vitro* was the same as that *in vivo* (Fig. 5M). In addition, GSH-Px activity, GSH content and GSH/GSSG ratio decreased and the content of GSSG increased significantly in EMB group and MPs group. In the the EMB+MPs group, the above indexes changed significantly (Fig. 5N). The above data confirm that EMB or/and MPs can induce oxidative stress, ROS overproduction, lipid peroxidation and GSH/GSSG system disorder.

3.6. Confirmation of the interaction among lysosomes, ROS, Fe^{2+}, and lipid peroxidation

To explore the relationship among lysosomes, ROS, Fe^{2+} and lipid peroxidation, we added the lysosome activator (EN6), lysosome inhibitor (CQ) and oxidative stress inhibitor (NAC) to EMB+MPs group. In Fig. 6A-B, the results of FerroOrange staining showed that, compared with the EMB+MPs group, the addition of CQ further increased the red fluorescence intensity of Fe^{2+} ($P < 0.05$), while EN6 or NAC decreased the fluorescence intensity of Fe^{2+}, but there was no significant difference between EMB+MPs and EMB+MPs+NAC groups ($P > 0.05$). In Fig. 6C-D, the results of DCFH-DA staining showed that compared with the EMB+MPs group, the ROS content in EMB+MPs+CQ group was further increased, and the ROS level was significantly decreased after adding EN6 or NAC, and the effect of NAC was better than EN6 ($P < 0.05$). In Fig. 6E-F, Lyso-tracker staining results showed that compared with the EMB+MPs group, CQ treatment could further reduce the number of lysosomes ($P < 0.05$), and adding EN6 or NAC could partially restore the number of lysosomes, and EN6 was better than NAC. In addition, C11 BODIPY 581/591 staining results showed that compared with the EMB+MPs group, the lipid peroxidation in EMB+MPs+CQ group was further aggravated, and the addition of EN6 or NAC significantly reduced the green lipid oxidation (Fig. 6G-I). These results indicate that lysosomes and iron overload mediate lipid peroxidation through ROS.

3.7. Effects of EMB or/and MPs exposure on iron metabolism and GPx4 expression

Based on the production of ROS and lipid peroxidation, we first explored the expression changes of EMB or/and MPs on ferroptosis marker gene (GPx4) and iron metabolism (Fig. 7A). In Fig. 7a, the mRNA levels of GPx4 and iron metabolism-related genes in carp midgut were screened from transcriptomics. The Fe^{2+} content in EMB group and MPs group increased, compared with the control group ($P > 0.05$), and the Fe^{2+} content in EMB+MPs group increased about twice (Fig. 7b). In Fig. 7c-e, the expressions of iron transport genes (TFR, TF and DMT1) and iron utilization genes (FTH and FTL) were up-regulated in MPs group or EMB group ($P < 0.05$), while the expression of iron efflux gene (FPN) was down-regulated, and these indexes changes were more obvious in EMB+MPs group. For the expression of GPx4, we discovered that the level of GPx4 in the single exposure group decreased significantly ($P < 0.05$) from the levels of IF (Fig. 7f), mRNA (Fig. 7g) and protein (Fig. 7h), and the level of GPx4 in EMB+MPs group further decreased to the lowest level. These results prove that EMB or/and MPs induce iron metabolism abnormality and ferroptosis in carp midgut.

Subsequently, the effects of EMB or/and MPs exposure on iron metabolism and GPx4 expression were verified on EPC cells *in vitro* (Fig. 7B). First, we detected the content of Fe^{2+} by the bipyridine method and FerroOrange staining method. Compared with the C group, the Fe^{2+} content and fluorescence intensity in EMB group or MPs group

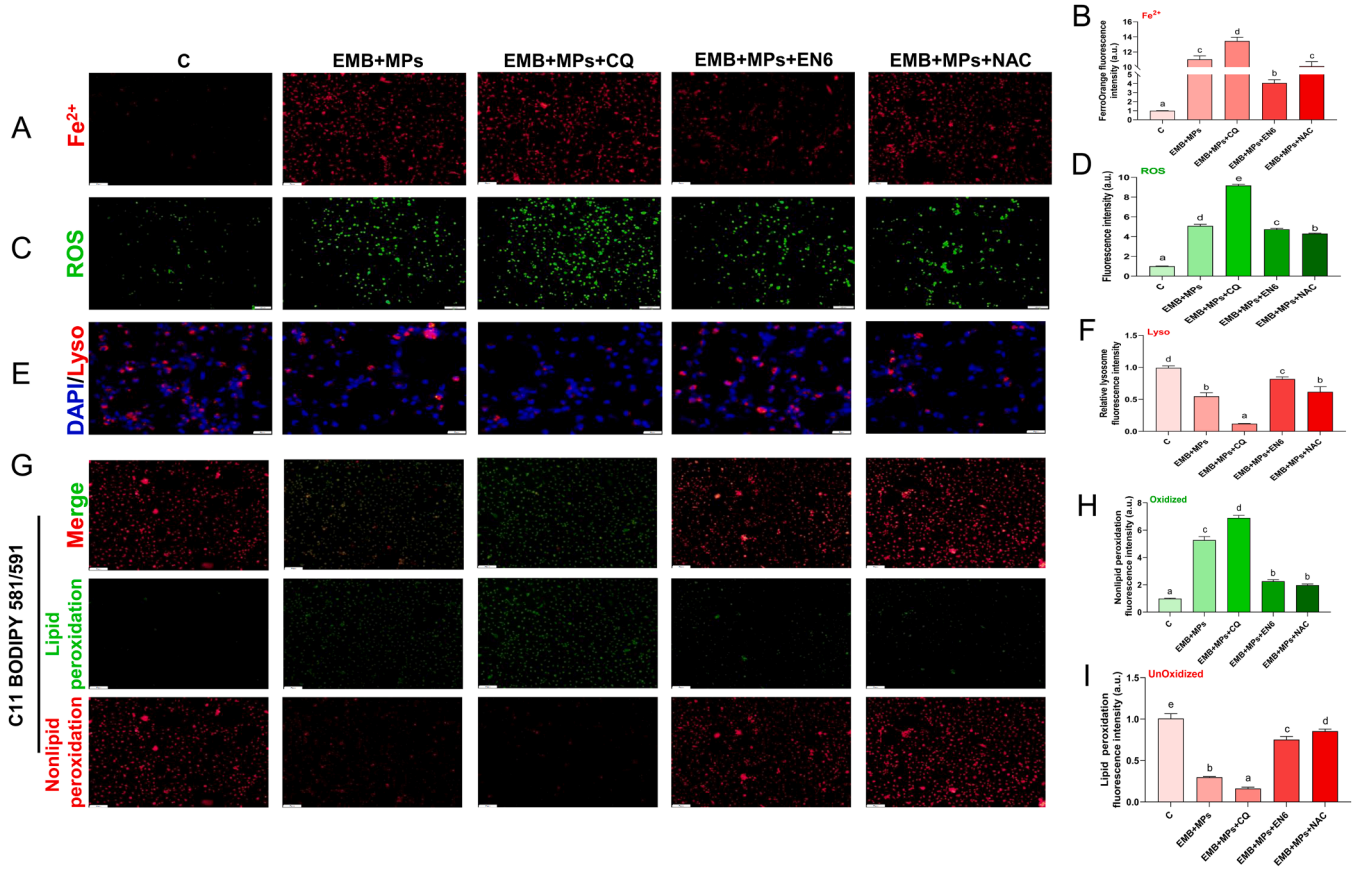

Fig. 6. Confirmation of the relationship among lysosome, ROS, Fe^{2+} and lipid peroxidation (A, B) The detection and quantification of Fe^{2+} content in EPC cells by FerroOrange (1 μM) staining (n=3). (C, D) The detection of ROS level (Green) in EPC cells by DCFH-DA staining (n=3). (E, F) Lyso-tracker and Hoechst 33342 stained the lysosome and nuclei of EPC cells (n=3). (G) The detection of lipid peroxidation in EPC cells by C11 BODIPY 581/591 staining (n=3). (H, I) Quantification of lipid peroxidation and non-lipid peroxidation fluorescence intensity in EPC cells (n=3). Scale, 100 μm.

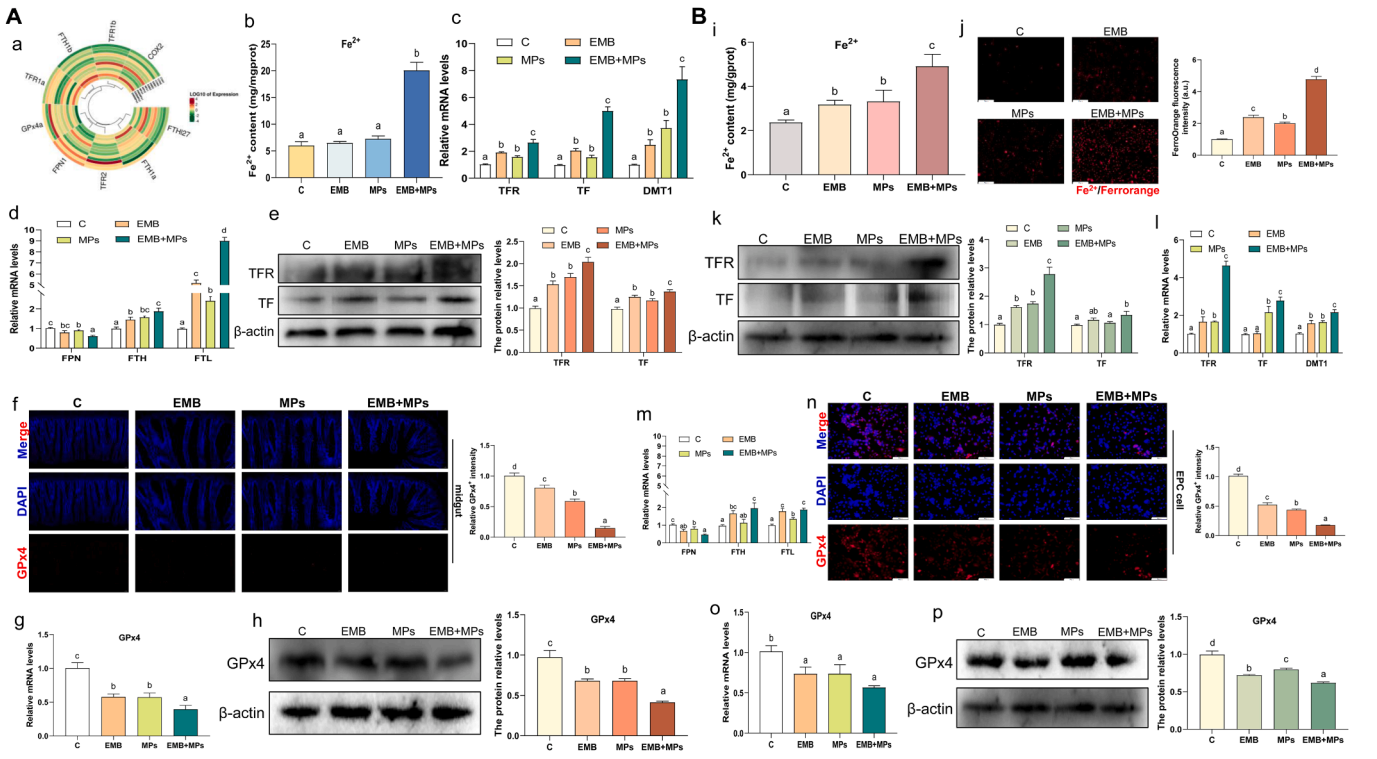

Fig. 7. Effects of EMB or/and MPs exposure on iron metabolism and GPx4 expression *in vivo* and *in vitro*

A (a) The cyclic thermogram of ferroptosis related gene expression in transcriptomics (n=3). (b) The detection results of Fe^{2+} (mg/mgprot) content in carp midgut (n=4). (c) The mRNA levels of TFR, TF, and DMT1 (n=3). (d) The mRNA levels of FPN, FTH, and FTL (n=3). (e) The protein expression and quantitative graphs of TFR and TF (n=3). (f) IF results and quantification of GPx4 (Red) in carp midgut. DAPI (Blue) stained nuclei (Scale, 50 μm). (g, h) The mRNA and protein levels of GPx4 in carp midgut (n=3).

B (i) The detection results of Fe^{2+} (mg/mgprot) content in EPC cells (n=4). (j) The detection and quantification of Fe^{2+} content in EPC cells by FerroOrange staining (Scale, 100 μm) (n=3). (k) The protein expression and quantitative graphs of TFR and TF (n=3). (l) The mRNA levels of TFR, TF, and DMT1 (n=3). (m) The mRNA levels of FPN, FTH, and FTL (n=3). (n) IF results and quantification of GPx4 (Red) in EPC cells. DAPI (Blue) stained nuclei (Scale, 100 μm). (o, p) The mRNA and protein levels of GPx4 in EPC cells (n=3).

were significantly enhanced ($P < 0.05$), while the EMB+MPs treatment group was further increased (Fig. 7i-j). In Fig. 7k-m, the EMB+MPs group had higher levels of TFR, TF, DMT1, FTH, and FTL and lower level of FPN expression than the MPs group or EMB group ($P < 0.05$). Adding lysosome activator EN6 (Fig. S1A and S1C) and oxidative stress inhibitor NAC (Fig. S1B and S1D) can significantly alleviate the abnormal expression of iron metabolism-related genes caused by EMB and MPs exposure. In addition, compared with the C group, the levels of $GPx4^{+}$ red fluorescence (Fig. 7n), transcription (Fig. 7o) and protein (Fig. 7p) in EMB group or MPs group were significantly decreased ($P < 0.05$), while the changes in EMB+MPs exposure group were decreased to the lowest. Compared with the EMB+MPs group, the levels of GPx4 mRNA (Fig. S1E and S1G), protein (Fig. S1F and S1H) and fluorescence intensity (Fig. S1I and S1J) in EMB+MPs+EN6 group and EMB+MPs+NAC group recovered obviously ($P < 0.05$). These data indicate that the lysosome/ROS axis participates in iron metabolism abnormality and ferroptosis caused by EMB or/and MPs exposure.

3.8. *Effects of EMB or/and MPs exposure on gap junction, inflammation and immune function*

First, we investigated the influence of EMB or/and MPs treatment on the midgut tissue of carp (Fig. 8A). GSEA analysis results showed that EMB or/and MPs regulated immune response, inflammatory response, gap junction biological process and the response of immune cells (T cells, macrophages, B cells and lymphocytes) (Fig. 8a). Based on the above results of GSEA enrichment, we screened the genes related to intestinal tight indirect, inflammation and immune response and made a circular thermogram to further select the subsequent detection genes (Fig. 8b). In Fig. 8c-d, the fluorescence intensity of connexin (Cx43) in EMB group or MPs group was declined ($P < 0.05$), and it was further significantly decreased in EMB+MPs group. Except for Cx43, the mRNA and protein levels of ZO-1, Occludin, Mucin2, and Claudin from low to high were EMB+MPs group, single exposure group and C group (Fig. 8e-f). In addition, compared with the control group, the transcription and fluorescence intensity levels of inflammatory factors (TNF-α and IL-1β) in EMB or MPs treatment group were significantly increased (Fig. 8g-h), and the changes in EMB+MPs group was further increased ($P < 0.05$). Furthermore, the mRNA levels of IFN-γ, IL-2, and IL-10, immunoglobulins (IgM, IgG, and IgD) and the protein expression of IFN-γ and IL-2 decreased with EMB or MPs treatment. The expression of the above indexes in EMB+MPs exposure group was further decreased (Fig. 8i-j). These results indicate that EMB or/and MPs induce intestinal barrier damage, inflammation and immune disorder in carp midgut.

On EPC cells *in vitro*, we verified the effects of EMB or/and MPs on inflammation, immune function and intestinal tight junction (Fig. 8B). The fluorescence intensity and mRNA level of IL-1β and TNF-α in EMB group or MPs group, compared with the control group, were significantly increased (Fig. 8k-l), and further increased in EMB+MPs group ($P < 0.05$). Compared with the EMB+MPs group, the transcription degree of TNF-α and IL-1β in EMB+MPs+EN6 group (Fig. 8m) and EMB+MPs+NAC group (Fig. S2A) decreased significantly ($P < 0.05$). Furthermore, the expression of immune-related genes (immunoglobulins, IFN-γ, IL-2, and IL-10) decreased after EMB or MPs exposure, and these genes were further down-regulated after combined exposure (Fig. 8n-o). Adding EN6 (Fig. 8m and 8p) or NAC (Fig. S2B-D)

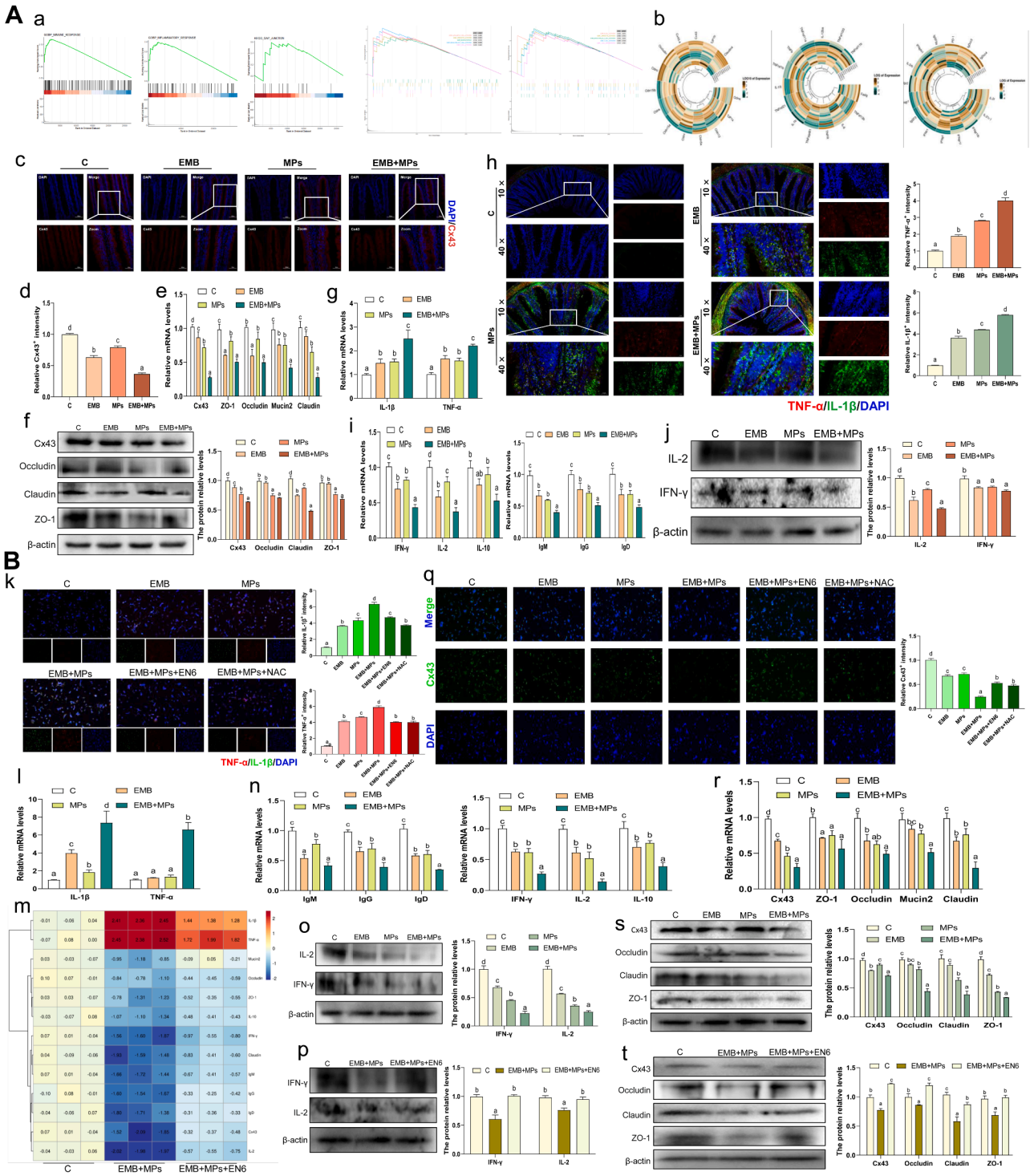

Fig. 8. Effects of EMB and/or MPs on tight junction, immune and inflammation *in vivo* and *in vitro*

A (a) The results of GSEA enrichment in the transcriptomics of carp midgut. (b) The cyclic thermogram of tight junction, immunity, and inflammation related gene expression in transcriptomics (n=3). (c, d) IF results and quantification of Cx43 (Red) in carp midgut. DAPI (Blue) stained nuclei (Scale, 50 μm and 100 μm). (e) The mRNA levels of Cx43, ZO-1, Occludin, Mucin2, and Claudin (n=3). (f) The protein expression and quantitative of Cx43, ZO-1, Occludin, and Claudin (n=3). (g) The mRNA levels of IL-1β and TNF-α (n=3). (h) IF results and quantification of IL-1β (Green) and TNF-α (Red) in carp midgut. DAPI (Blue) stained nuclei (Scale, 20 μm and 100 μm). (i) The mRNA levels of IFN-γ, IL-2, IL-10, IgM, IgG, and IgD (n=3). (j) The protein expression and quantitative of IL-2 and IFN-γ (n=3).

B (k) IF results and quantification of IL-1β (Green) and TNF-α (Red) in EPC cells. DAPI (Blue) stained nuclei (Scale, 50 μm). (l) The mRNA levels of IL-1β and TNF-α (n=3). (m) The heat map of IL-1β, TNF-α, IFN-γ, IL-2, IL-10, IgM, IgG, IgD, Cx43, ZO-1, Occludin, Mucin2, and Claudin mRNA levels in C, EMB+MPs, and EMB+MPs+NAC groups (n=3). (n) The mRNA levels of IFN-γ, IL-2, IL-10, IgM, IgG, and IgD (n=3). (o) The protein expression and quantitative of IL-2 and IFN-γ (n=3). (p) The protein expression and quantitative of IL-2 and IFN-γ after adding EN6 (n=3). (q) IF results and quantification of Cx43 (Green) in EPC cells. DAPI (Blue) stained nuclei (Scale, 50 μm). (r) The mRNA levels of Cx43, ZO-1, Occludin, Mucin2, and Claudin (n=3). (s) The protein expression and quantitative of Cx43, ZO-1, Occludin, and Claudin (n=3). (t) The protein expression and quantitative of Cx43, ZO-1, Occludin, and Claudin after adding EN6 (n=3).

significantly alleviated the down-regulation of the above indexes induced by the combined treatment of EMB and MPs ($P < 0.05$). In addition, compared with C group, the green fluorescence of $Cx43^+$ in EMB or MPs exposure group declined significantly, while compared with EMB+MPs, the levels of $Cx43^+$ in EMB+MPs+EN6 group and EMB+MPs+NAC group increased significantly, and the effect of EN6 was better than that of NAC (Fig. 8q). The transcription and protein levels of Cx43, ZO-1, Occludin, Mucin2, and Claudin in the joint treatment group were lower than those in EMB or MPs group (Fig. 8r-s) ($P < 0.05$). The addition of EN6 (Fig. 8m and 8t) or NAC (Fig. S2E-F) can alleviate the abnormal expression of the intestinal tight junction gene caused by joint exposure. These results show that the lysosome/ROS axis is involved in adjusting the intestinal barrier damage, inflammation and immune disorder induced by EMB or/and MPs exposure.

4. Discussion

Although there are many studies on the toxicity mechanism of MPs, we know little about the toxicity mechanism of EMB and the toxicity of EMB and MPs combined exposure in aquatic organisms. As we all know, the intestine is the most important organ of "immune detoxification" (Niu, Guan et al. 2023), which will lead to immune and inflammatory reactions through barrier damage. By collecting previous research data, we found that EMB and MPs had a co-occurrence in geographical distribution, and both pesticides (EMB. et al) and MPs can cause inflammation and immune response in multiple tissues and organs (Anbumani, Kakkar et al. 2018, Kilercioglu, Ay et al. 2020, Kumar, Swain et al. 2022). Based on these data, our study explored the mechanism of immune disorder and inflammation in carp midgut caused by EMB or/and MPs exposure. The data revealed that EMB or MPs exposure induced the midgut cilia to become less and shorter, the intestinal tight junction and the expression of immune-related genes decreased, and the level of inflammation factors increased. In addition, single exposure also caused lysosome damage, excessive ROS production, abnormal iron metabolism, lipid peroxidation and ferroptosis. Combined exposure aggravated the changes in the above indexes, and adding EN6 or NAC could alleviate this phenomenon.

200 μm PS-MPs specifically changed the lysosomes of the intestinal macrophages in zebrafish (Gu, Liu et al. 2020). MPs treatment with 24, 48 and 96 μg/mL PVC for 3 h can induce ROS formation and lysosomal membrane damage in human blood lymphocytes (Salimi, Alavehzadeh et al. 2022). 100 nm NPs and 1 μm MPs were deposited in lysosomes of embryonic zebrafish fibroblast cells, which caused lysosomes to be acidified (MPs) and alkalized (NPs). Furthermore, after lysosomes break and escape, ROS is induced to produce significantly and autophagy is activated (Yang and Wang 2022). EMB exposure increases the oxidative stress of zebrafish heart through excessive ROS and abnormal activity of antioxidant enzymes (Lu, Wang et al. 2022). However, there is no literature about the effect of EMB on lysosomes. On the carp midgut and EPC cells in this study, we discovered for the first time that EMB or MPs exposure caused lysosome damage, while the combined exposure further aggravated the damage by detecting the lysosomal acidification (ATP6V1A, ATP6V1C2 and ATP6V1H), enzyme activities (NAG and ACP), lysosomal permeability (CTSB) and lysosomal number (Lyso--tracker). Through the decrease of antioxidant enzyme activity and the increase of ROS level, combined exposure has a higher level of oxidative stress than single exposure. To explore whether lysosomes or ROS first responded to EMB or/and MPs toxicity, we added EN6, CQ and NAC to the EMB+MPs group, and found that the lysosome/ROS axis was dominant compared with the ROS/lysosome axis. In addition, it is due to the high enrichment of iron metabolism and lysosomes by transcriptomics and the bridge function of NCOA4 connecting lysosomes and iron metabolism (Zhang, Chen et al. 2021). In our study, EMB or/and MPs exposure induced abnormal iron metabolism, which led to the increase of Fe^{2+} content. Compared with NAC treatment, the addition of EN6 had a more significant effect on alleviating the excessive production of Fe^{2+}. This shows that EMB or/and MPs exposure leads to iron overload through lysosomal damage, which significantly increases the intracellular Fe^{2+} content. We found similar results in MPs-related research (Cheng, Zhou et al. 2023), but this study was the first time that EMB exposure caused abnormal intracellular Fe^{2+} content and iron metabolism disorder through iron overload. The above results manifest that EMB or/and MPs exposure can activate the lysosome/ROS axis, and lead to the increase of intracellular Fe^{2+} content through iron overload.

There are three key pathways for ferroptosis, namely iron overload, inactivation of GPx4 and lipid peroxidation (Xu, Cui et al. 2023). Raw materials for GSH synthesis will be transported into cells through SLC7A11 and SLC3A2 (Zhang, Zheng et al. 2022). Exposure to 1 mg/L MPs induced lower levels of glutathione-s transferase (GST) in freshwater bivalve (*Unio totumidus*), but higher levels of GSH and GSSG (Martyniuk, Khoma et al. 2022). Exposure to 250 mg/10 mL MPs (8 μm) for 21 days induced lipid peroxidation in carp intestine, and the expressions of ferroptosis-related factors COX-2 and ACSL4 were up-regulated, while the expressions of SLC7A11 and GPx4 were down-regulated (Xu, Cui et al. 2023). Echoing previous studies, we found that MPs exposure induced GSH/GSSG system disorder, lipid peroxidation and ferroptosis in carp midgut and EPC cells. Furthermore, combined exposure of MPs and pesticide imidacloprid activates the ferroptosis pathway by increasing ROS and MDA content (Fu, Zhu et al. 2023). Avermectins (ivermectin (Huang, He et al. 2021) and avermectin (Gur, Kandemir et al. 2022)) can cause GSH metabolism, lipid peroxidation and ferroptosis. Therefore, it was found for the first time that EMB exposure induced GSH/GSSG system disorder, lipid peroxidation and ferroptosis in carp intestine, and it would have a joint toxic effect with MPs. By adding EN6 and NAC, we confirmed that the lysosome/ROS axis was involved in regulating lipid peroxidation and ferroptosis in carp midgut induced by EMB or/and MPs exposure. In addition, lysosomal injury and iron overload have been reported to increase ROS and drive ferroptosis (Patricia, Antioxidants et al. 2012, Cao, Zhao et al. 2016, Rizzollo, More et al. 2021). Therefore, by adding EN6, CQ and NAC, it was confirmed that lysosomal injury would lead to lipid peroxidation and iron overload through excessive ROS production, and lysosomes would also regulate the increase of intracellular Fe^{2+} content through the expression of NCOA4, so excessive Fe^{2+} would also lead to ROS production. However, whether ROS is involved in affecting lysosome damage and Fe^{2+} content, we think there must be this process. However, on the premise of EMB or/and MPs treatment, the lysosome/ROS axis dominates the response.

The integrity of intestinal cilia and tight junction will affect the intestinal immune barrier, thus causing inflammatory damage. After exposure to 0.1% (w/w) MPs in the diet for 30 days, 67% of European perch (*Dicentrarchuslabrax*) had its connective tissue widened, cilia shortened and swollen, intestinal cells vacuolated, and distal intestinal goblet cells increased (Pedà, Caccamo et al. 2016). Exposure to a 3 μg/kg EMB diet for 7 days induced intestinal villi necrosis, mucinous degeneration, inflammation and epithelial degeneration in *Nile tilapia* (Julinta, Abraham et al. 2020). In this study, EMB or MPs exposure caused the intestinal cilia to decrease and shorten obviously, and the structural integrity of midgut tissue was destroyed. Combined exposure of EMB and MPs further aggravated midgut injury and inflammatory cell infiltration. Studies have shown that MPs exposure induces the dysfunction of intestinal immune cells (Gu, Liu et al. 2020) and the increase of inflammatory cytokines (TNF-α, IL-1β, IL-6) (Xu, Cui et al. 2023). MPs also has a joint toxic effect with other poisons. For example, the joint exposure of MPs and cadmium reduced the expression of Cx43 protein in mouse testis (Hassine, Venditti et al. 2023); The combined treatment of MPs and glyphosate induced the decreased levels of tight junction genes (Occludin, Claudin, and ZO-1) in the brain (Chen, Rao et al. 2022). EMB exposure led to the decrease of IgG and IgM concentration, C3 activity and the down-regulation of IL-1β, and TNF-α in erum of *L. rohita*, rainbow trout and rats (Ei-Sheikh, Galal et al. 2015, Kilercioglu, Ay et al. 2020, Kumar, Swain et al. 2022). Although some studies have found that

EMB can damage intestinal cilia and structure (Julinta, Abraham et al. 2020), the effects on intestinal tight junction have not been reported. Abamectin exposure led to the down-regulation levels of tight junction genes (ZO-1 and Occludin) in carp brain, and the structure of blood-brain barrier was destroyed (Zhang, Dong et al. 2022). In this study, we found that EMB or MPs exposure induced the gap junction and tight junction disorder, decreased immune function and increased inflammation in carp midgut, and the above changes were more significant in combination exposure. By adding EN6 and NAC to EPC cells, we confirmed that the lysosome/ROS axis was involved in the process of tight junction, immunity and inflammation. Indeed, some studies have found that the ferroptosis inhibitor (Fer-1) can reduce nicotine-induced testicular barrier damage by regulating the expressions of ZO-1, Claudin, Occludin and Cx43 (Zhang, Cheng et al. 2023). The above results demonstrate that EMB or/and MPs exposure lead to tight junction disorder of carp midgut through the lysosome/ROS/ferroptosis axis, thus causing immune disorder and inflammation.

5. Conclusion

In a word, our data identifies a new potential mechanism of intestinal injury induced by EMB or/and MPs exposure in carp. EMB or MPs exposure alone causes lysosome damage and excessive ROS production, thus activating ferroptosis pathways (iron overload, GSH/GSSG system and lipid peroxidation), and further causing intestinal tight junction disorder, immune disorder and inflammation. This series of reactions caused by joint exposure is more significant than that induced by single exposure. At the same time, this study discovers some new toxic effects of EMB for the first time, that is, EMB exposure will cause lysosome damage, lipid peroxidation, ferroptosis and tight junction disorder. The results of this study have important reference significance for predicting and studying the exposure of EMB and MPs to other animals and humans, and provide a theoretical basis for interdisciplinary research.

Compliance with Ethics Requirements

All procedures used in this research were approved by the Institutional Animal Care and Use Committee of Northeast Agricultural University (SRM-11).

CRediT authorship contribution statement

Xu Shi: Writing – original draft, Software, Methodology, Investigation, Conceptualization. **Tong Xu:** Writing – review & editing, Visualization. **Meichen Gao:** Visualization, Validation. **Yanju Bi:** Visualization, Validation. **Jiaqi Wang:** Visualization. **Yilin Yin:** Visualization. **Shiwen Xu:** Writing – review & editing, Resources, Funding acquisition.

Declaration of competing interest

The authors declare that they have no known competing financial interests or personal relationships that could have appeared to influence the work reported in this paper.

Data availability

Data will be made available on request.

Funding

This study was supported by the National Natural Science Foundation of China (U22A20524) and the Natural Science Foundation of Heilongjiang Province (ZD2023C002).

Acknowledgements

The authors extend their sincere thanks to the members of the Veterinary Internal Medicine Laboratory, Key Laboratory of Experimental Animals and Embryo Biotechnology Laboratory of College of Life Sciences of Northeast Agricultural University, Northeast Agricultural University.

Supplementary materials

Supplementary material associated with this article can be found, in the online version, at doi:10.1016/j.watres.2024.121660.

Reference

Anbumani, S., Kakkar, P.J.E.S., Research, P., 2018. Ecotoxicological effects of microplastics on biota: a review 25 (15), 14373–14396.

Bobori, D., Feidantsis, K., Dimitriadi, A., Datsi, N., Ripis, P., Kalogiannis, S., Sampsonidis, I., Kastrinaki, G., Ainali, N., Lambropoulou, D., Kyzas, G., Koumoundouros, G., Bikiaris, D., j. o. m. s. Kaloyianni, M.J.I., 2022. Dose-Dependent Cytotoxicity of Polypropylene Microplastics (PP-MPs) in Two Freshwater Fishes 23 (22), 13878.

Cao, X., Zhao, M., Li, D., Xing, Y., Zhang, Y., Chen, J., He, X., Cui, R., Meng, J., Xiao, X., Mu, J., Jiang, Y., Wu, R.J.Z.y.x.z.z., 2016. [Establishment of macrophage model of iron overload in vitro and the injury induced by oxidative stress on macrophage with iron overload] 96 (2), 129–133.

Chen, J., Rao, C., Yuan, R., Sun, D., Guo, S., Li, L., Yang, S., Qian, D., Lu, R., o. t. t. e. Cao, X.J.T.S., 2022. Long-term exposure to polyethylene microplastics and glyphosate interferes with the behavior, intestinal microbial homeostasis, and metabolites of the common carp (Cyprinus carpio L.) 814, 152681.

Cheng, B., Van Smeden, J., Deneer, J., Belgers, D., Foekema, E., Roessink, I., Matser, A., Van den Brink, P.J.E., e. safety, 2020. The chronic toxicity of emamectin benzoate to three marine benthic species using microcosms 194, 110452.

Cheng, W., Zhou, Y., Chen, H., Wu, Q., Li, Y., Wang, H., Feng, Y., Wang, Y.J.T.S.o.t.t.e., 2023. The iron matters: Aged microplastics disrupted the iron homeostasis in the liver organoids 906, 167529.

Compa, M., Ventero, A., Iglesias, M., Deudero, S.J.M.P.B., 2018. Ingestion of microplastics and natural fibres in Sardina pilchardus (Walbaum, 1792) and Engraulis encrasicolus (Linnaeus, 1758) along the Spanish Mediterranean coast 128, 89–96.

Del Piano, F., Lama, A., Piccolo, G., Addeo, N., Iaccarino, D., Fusco, G., Riccio, L., De Biase, D., Mattace Raso, G., Meli, R., Ferrante, M.J.T.S.o.t.t.e., 2023. Impact of polystyrene microplastic exposure on gilthead seabream (Sparus aurata Linnaeus, 1758): Differential inflammatory and immune response between anterior and posterior intestine 879, 163201.

Devriese, L.I., Van, d.M., Myra, D, Maes, T., Bekaert, K., Paul-Pont, I., Frere, L., Robbens, J., Vethaak, A.D.J.M.P.B., 2015. Microplastic contamination in brown shrimp (Crangon crangon, Linnaeus 1758) from coastal waters of the Southern North Sea and Channel area 98 (1-2), 179–187.

Doll, S., Proneth, B., Tyurina, Y.Y., Panzilius, E., Kobayashi, S., Ingold, I., Irmler, M., Beckers, J., Aichler, M., Walch, A.J.N.c.b., 2016. ACSL4 dictates ferroptosis sensitivity by shaping cellular lipid composition 13 (1), 91–98.

Ei-Sheikh, E.S.A., Galal, A.A.A.J.E.T., Pharmacology, 2015. Toxic effects of sub-chronic exposure of male albino rats to emamectin benzoate and possible ameliorative role of Foeniculum vulgare essential oil 39 (3), 1177–1188.

Fu, H., Zhu, L., Mao, L., Zhang, L., Zhang, Y., Chang, Y., Liu, X., Jiang, H.J.T.S.o.t.t.e., 2023. Combined ecotoxicological effects of different-sized polyethylene microplastics and imidacloprid on the earthworms (Eisenia fetida) 870, 161795.

Gall, S.C., Thompson, R.C.J.M.P.B., 2015. The impact of debris on marine life 92 (1-2), 170–179.

Gao, M., Yang, N., Lei, Y., Zhang, W., Liu, H., Lin, H.J.F., s. immunology, 2022. Tannic acid antagonizes atrazine exposure-induced autophagy and DNA damage crosstalk in grass carp hepatocytes via NO/iNOS/NF-κB signaling pathway to maintain stable immune function 131, 1075–1084.

Gao, M., Zhu, H., Guo, J., Lei, Y., Sun, W., Lin, H.J.F., s. immunology, 2022. Tannic acid through ROS/TNF-α/TNFR 1 antagonizes atrazine induced apoptosis, programmed necrosis and immune dysfunction of grass carp hepatocytes 131, 312–322.

Gu, J., Guo, L., Hu, J., Ji, G., o. t. t. e. Yin, D.J.T.S., 2023. Potential adverse outcome pathway (AOP) of emamectin benzoate mediated cardiovascular toxicity in zebrafish larvae (Danio rerio) 900, 165787.

Gu, W., Liu, S., Chen, L., Liu, Y., Gu, C., Ren, H.Q., Wu, B.J.E.S., T, ES, 2020. Single-Cell RNA Sequencing Reveals Size-Dependent Effects of Polystyrene Microplastics on Immune and Secretory Cell Populations from Zebrafish Intestines 54 (6), 3417–3427.

Gur, C., Kandemir, O., Kandemir, F.J.E.t, 2022. Investigation of the effects of hesperidin administration on abamectin-induced testicular toxicity in rats through oxidative stress, endoplasmic reticulum stress, inflammation, apoptosis, autophagy, and JAK2/STAT3 pathways 37 (3), 401–412.

Hassine, M., Venditti, M., Rhouma, M., Minucci, S., Messaoudi, I.J.E.s., p. r. international, 2023. Combined effect of polystyrene microplastics and cadmium on rat blood-testis barrier integrity and sperm quality 30 (19), 56700–56712.

Huang, H., He, Q., Guo, B., Xu, X., Wu, Y., Li, X.J.D.d., development and therapy, 2021. Progress in Redirecting Antiparasitic Drugs for Cancer Treatment 15, 2747–2767.

Brooks, J, S., Ruus, J.T, Kringstad, Rundberget, Environment, L.J.T.S.o.t.T., 2019. Bioaccumulation of selected veterinary medicinal products (VMPs) in the blue mussel (Mytilus edulis) 655, 1409–1419.
Julinta, R., Abraham, T., Roy, A., Singha, J., Bardhan, A., Sar, T., Patil, P., Kumar, K.J.E. t., pharmacology, 2020. Safety of emamectin benzoate administered in feed to Nile tilapia Oreochromis niloticus (L.) 75, 103348.
Kang, H., Byeon, E., Jeong, H., Kim, M., Chen, Q., o. h. m. Lee, J.J.J., 2021. Different effects of nano- and microplastics on oxidative status and gut microbiota in the marine medaka Oryzias melastigma 405, 124207.
Kilercioglu, S., Ay, O., Oksuz, H., Yilmaz, M.B.J.M.B.R., 2020. The effects of the neurotoxic agent emamectin benzoate on the expression of immune and stress-related genes and blood serum profiles in the Rainbow trout 47 (7), 5243–5251.
Krainz, T., Gaschler, M.M., Lim, C., Sacher, J.R., Wipf, P.J.A.C.S., 2011. A Mitochondrial-Targeted Nitroxide Is a Potent Inhibitor of Ferroptosis 2 (9), 653.
Kumar, V., Swain, H., Das, B., Roy, S., Upadhyay, A., Ramteke, M., Kole, R., Banerjee, H. J.T.r., 2022. Labeo rohitaAssessment of the effect of sub-lethal acute toxicity of Emamectin benzoate in using multiple biomarker approach 9, 102–110.
Li, Y., Hu, J., Cheng, C., Xu, F., Au, R., Zhu, L., Shen, H.J.E.-b.c., a. m. eCAM, 2022. Baicalin Ameliorates DSS-Induced Colitis by Protecting Goblet Cells through Activating NLRP6 Inflammasomes 2022, 2818136.
Liu, Y., Sun, H., Wang, X., Chang, H., Wang, S.J.M., 2023. Dissipation Dynamic, Residue Distribution and Risk Assessment of Emamectin Benzoate in Longan by High-Performance Liquid Chromatography with Fluorescence Detection 28 (8), 3346.
Liu, Z., Wang, W., Liu, Y., Wu, T., Teng, G.J.Z.y.x.z.z., 2021. [Elafin-expressing probiotic Escherichia coli Nissle 1917 protects against experimental colitis] 101 (46), 3819–3824.
Lu, J., Wang, W., Xu, W., Zhang, C., Zhang, C., Tao, L., Li, Z., Zhang, Y.J.T.S.o.t.t.e., 2022. Induction of developmental toxicity and cardiotoxicity in zebrafish embryos by Emamectin benzoate through oxidative stress 825, 154040.
Martyniuk, V., Khoma, V., Matskiv, T., Baranovsky, V., Orlova-Hudim, K., Gylytė, B., Symchak, R., Matciuk, O., Gnatyshyna, L., Manusadžianas, L., Stoliar, O.J.C.b., p. Toxicology and p. CBP, 2022. Indication of the impact of environmental stress on the responses of the bivalve mollusk Unio tumidus to ibuprofen and microplastics based on biomarkers of reductive stress and apoptosis 261, 109425.
Miao, Z., Miao, Z., Feng, S., Xu, S.J.F., s. immunology, 2023. Chlorpyrifos-mediated mitochondrial calcium overload induces EPC cell apoptosis via ROS/AMPK/ULK1 141, 109053.
Miao, Z., Miao, Z., Liu, M., Xu, S.J.F., s. immunology, 2022. Melatonin ameliorates imidacloprid-induced intestinal injury by negatively regulating the PGN/P38MAPK pathway in the common carp (Cyprinuscarpio) 131, 1063–1074.
Niu, C., Guan, J., Meng, G., Zhou, Y., Wei, Y.J.S.w.g.c.x.b.C.j.o.b., 2023. Drosophila[The regulatory relationship between RagA and Nprl2 in gut development] 39 (4), 1747–1758.
Ouyang, M., Liu, J., Wen, B., Huang, J., Feng, X., Gao, J., Chen, Z.J.J.o.h.m., 2021. Ecological stoichiometric and stable isotopic responses to microplastics are modified by food conditions in koi carp 404, 124121.
Patricia, B.J.Antioxidants, signaling, r., 2012. Lysosomal function and dysfunction: mechanism and disease 17 (5), 766–774.
Pedà, C., Caccamo, L., Fossi, M., Gai, F., Andaloro, F., Genovese, L., Perdichizzi, A., Romeo, T., p. Maricchiolo, G.J.E., 2016. Intestinal alterations in European sea bass Dicentrarchus labrax (Linnaeus, 1758) exposed to microplastics: Preliminary results 212, 251–256.
Rico, A., Redondo-Hasselerharm, P., Vighi, M., Waichman, A., Nunes, G., de Oliveira, R., Singdahl-Larsen, C., Hurley, R., Nizzetto, L., r. Schell, T.J.W., 2023. Large-scale monitoring and risk assessment of microplastics in the Amazon River 232, 119707.
Rizzollo, F., More, S., Vangheluwe, P., i. b. s. Agostinis, P.J.T., 2021. The lysosome as a master regulator of iron metabolism 46 (12), 960–975.
Salimi, A., Alavehzadeh, A., Ramezani, M., Pourahmad, J.J.T., Health, I., 2022. Differences in sensitivity of human lymphocytes and fish lymphocytes to polyvinyl chloride microplastic toxicity 38 (2), 100–111.
Shi, X., Zhu, W., Chen, T., Cui, W., Li, X., Xu, S.J.F., s. immunology, 2022. Paraquat induces apoptosis, programmed necrosis, and immune dysfunction in CIK cells via the PTEN/PI3K/AKT axis 130, 309–316.
St-Hilaire, S., Cheng, T.H., Chan, S.C.H., Leung, C.F., Gomes, G.B.J.F.i.V.S., 2021. Emamectin Benzoate Treatment of Hybrid Grouper Infected With Sea Lice in Hong Kong 8 (646652), 1–9.
Subramanian, S., Geng, H., Tan, X.D.J.S.l.x.b., 2020. Cell death of intestinal epithelial cells in intestinal diseases 72 (3), 308–324.
Tan, H., Li, Q., Zhang, H., Wu, C., Zhao, S., Deng, X., Li, Y.J.T.S.o.t.t.e., 2020. Pesticide residues in agricultural topsoil from the Hainan tropical riverside basin: Determination, distribution, and relationships with planting patterns and surface water 722, 137856.
Tan, H., Zhang, H., Wu, C., Wang, C., Li, Q.J.E.p., 2021. Pesticides in surface waters of tropical river basins draining areas with rice-vegetable rotations in Hainan, China: Occurrence, relation to environmental factors, and risk assessment 283, 117100.
Wang, K., Liu, H., Sun, W., Guo, J., Jiang, Z., Xu, S., Miao, Z.J.A.t., 2023. Eucalyptol alleviates avermectin exposure-induced apoptosis and necroptosis of grass carp hepatocytes by regulating ROS/NLRP3 axis 264, 106739.
Wang, Y., Zhao, Y., Liang, H., Ma, C., Cui, N., Cao, H., Wei, W., Liu, Y.J.E.p., 2023. Single and combined effects of polyethylene microplastics and acetochlor on accumulation and intestinal toxicity of zebrafish (Danio rerio) 333, 122089.
Xu, T., Cui, J., Xu, R., Cao, J., Guo, M.J.A.t., 2023. Microplastics induced inflammation and apoptosis via ferroptosis and the NF-κB pathway in carp 262, 106659.
Yan, W., Hamid, N., Deng, S., Jia, P., Pei, D.J.J.o.h.m., 2020. Individual and combined toxicogenetic effects of microplastics and heavy metals (Cd, Pb, and Zn) perturb gut microbiota homeostasis and gonadal development in marine medaka (Oryzias melastigma) 397, 122795.
Yang, H., Sun, F., Liao, H., Guo, Y., Pan, T., Wu, F.J.W.r., 2023. The pollution of microplastics in sediments of the Yangtze River Basin: Occurrence, distribution characteristics, and basin-scale multilevel ecological risk assessment 243, 120322.
Yang, M., Wang, W.X.J.S.o.t.T.E., 2022. Differential cascading cellular and subcellular toxicity induced by two sizes of nanoplastics 829, 154593.
Yifeng, Lu, Yan, Zhang, Yongfeng, Deng, Wei, Jiang, Yanping, Z.J.E, Science and Technology, 2016. Uptake and Accumulation of Polystyrene Microplastics in Zebrafish (Danio rerio) and Toxic Effects in Liver 50 (7), 4054–4060.
Zhang, F., Li, D., Yang, Y., Zhang, H., Zhu, J., Liu, J., Bu, X., Li, E., Qin, J., Yu, N., Chen, L., Wang, X.J.T.S.o.t.t.e., 2022. Combined effects of polystyrene microplastics and copper on antioxidant capacity, immune response and intestinal microbiota of Nile tilapia (Oreochromis niloticus) 808, 152099.
Zhang, J., Chen, X., Hong, J., Tang, A., Liu, Y., Xie, N., Nie, G., Yan, X., Liang, M.J.S.C.L. s., 2021. Biochemistry of mammalian ferritins in the regulation of cellular iron homeostasis and oxidative responses 64 (3), 352–362.
Zhang, T., Dong, Z., Liu, F., Pan, E., He, N., Ma, F., Wang, G., Wang, Y., Dong, J.J.E., e. safety, 2022. Avermectin induces carp neurotoxicity by mediating blood-brain barrier dysfunction, oxidative stress, inflammation, and apoptosis through PI3K/Akt and NF-κB pathways 243, 113961.
Zhang, Y., Kong, C., Chi, H., Li, J., Qingfeng, Z.J.T.m., methods, 2019. Effect of a beta-cypermethrin and emamectin benzoate pesticide mixture on reproductive toxicity in male mice in a greenhouse environment 30 (2), 1–13.
Zhang, Y., Zheng, L., Deng, H., Feng, D., Hu, S., Zhu, L., Xu, W., Zhou, W., Wang, Y., Min, K., Zhou, Q., Chen, Y., Zhou, H., Yang, H., i. i. Lv, X.J.F., 2022. Electroacupuncture Alleviates LPS-Induced ARDS Through α7 Nicotinic Acetylcholine Receptor-Mediated Inhibition of Ferroptosis 13, 832432.
Zhang, Z., Cheng, J., Yang, L., Li, X., Hua, R., Xu, D., Jiang, Z., Li, Q.J.F.r.b., medicine, 2023. The role of ferroptosis mediated by Bmal1/Nrf2 in nicotine -induce injury of BTB integrity 200, 26–35.
Zhao, H., Wang, Y., Liu, Y., Yin, K., Wang, D., Li, B., Yu, H., Xing, M.J.E.s., technology, 2021. ROS-Induced Hepatotoxicity under Cypermethrin: Involvement of the Crosstalk between Nrf2/Keap1 and NF-κB/iκB-α Pathways Regulated by Proteasome 55 (9), 6171–6183.
Zhao, H., Zhang, Y., Hou, L., Lu, H., Zhang, Y., t. Xing, M.J.A., 2023. Effects of environmentally relevant cypermethrin and sulfamethoxazole on intestinal health, microbiome, and liver metabolism in grass carp 265, 106760.